A common molecular logic determines embryonic stem cell self-renewal and reprogramming

Sara-Jane Dunn[1,2,5], Meng Amy Li[2,5], Elena Carbognin[3], Austin Smith[2,4,6*] and Graziano Martello[3*]

[1]Microsoft Research, Cambridge, CB1 2FB, UK

[2]Wellcome Trust - Medical Research Council Cambridge Stem Cell Institute, University of Cambridge, Cambridge, CB2 1QR, UK

[3]Department of Molecular Medicine, University of Padua, Padua, 35131, Italy

[4]Department of Biochemistry, University of Cambridge, Cambridge, CB2 1GA, UK

[5]These authors contributed equally to this work and are listed in alphabetical order

[6]Lead contact

*Correspondence: austin.smith@cscr.cam.ac.uk (A.S.), graziano.martello@unipd.it (G.M.)

Abstract

During differentiation and reprogramming new cell identities are generated by reconfiguration of gene regulatory networks. Here we combined automated formal reasoning with experimentation to expose the logic of network activation during induction of naïve pluripotency. We find that a Boolean network architecture defined for maintenance of naïve state embryonic stem cells (ESC) also explains transcription factor behaviour and potency during resetting from primed pluripotency. Computationally identified gene activation trajectories were experimentally substantiated at single cell resolution. Contingency of factor availability explains the counterintuitive observation that Klf2, which is dispensable for ESC maintenance, is required during resetting. We tested 136 predictions formulated by the dynamic network, finding a predictive accuracy of 78.7%. Finally, we show that this network explains and predicts experimental observations of somatic cell reprogramming. We conclude that a common deterministic program of gene regulation is sufficient to govern maintenance and induction of naïve pluripotency. The tools exemplified here could be broadly applied to delineate dynamic networks underlying cell fate transitions.

Introduction

Over the last 10 years a multitude of protocols have been developed that allow the conversion of one cell type into another[1]. Most of these strategies rely on the forced expression of transcription factors (TFs) highly expressed by the target cell type that have either been chosen empirically or, recently, with the aid of computational tools such as CellNet or Mogrify[2–4]. Despite the large amount of transcriptomic data available for such

conversions, our understanding of the dynamics and logic followed by cells during reprogramming and transdifferentiation remains fragmentary.

The most studied cell fate transition is the generation of murine induced pluripotent stem cells (iPSCs) from somatic cells[5]. Bona fide iPSCs are, like murine embryonic stem cells (ESCs), competent to form blastocyst chimaeras, and are considered to occupy a state of naïve pluripotency similar to that in the pre-implantation embryo[6,7]. This unique identity is determined by a self-reinforcing interaction network of TFs. Experimental and computational efforts have led to circuitry mapping of the core TF program that maintains ESC self-renewal under defined conditions[8–14].

We previously applied a mathematical and computational modelling approach based on automated formal reasoning to elucidate the regulatory network architecture for self-renewing mouse ESCs[9,15]. A minimal interaction network of 12 components was found to recapitulate a large number of observations concerning naïve state maintenance, and successfully predicted non-intuitive responses to compound genetic perturbations[9].

Forced expression of several components of this core TF network in various cell types leads to a state of induced pluripotency[5,16–25]. Accumulating evidence suggests that cells progress through defined stages, with a final transition entailing the hierarchical activation and stabilisation of the naïve pluripotency TF network[16,17,26–33]. However, it is not clear if cells undergoing successful conversion follow a deterministic trajectory of gene activation,

defined by the naïve pluripotency TF network architecture, or if genes are activated in random sequence.

A tractable experimental system with which to investigate activation of naïve pluripotency is the resetting of post-implantation epiblast stem cells (EpiSCs)[34]. EpiSCs are related to gastrulation stage epiblast[35,36]. They represent a primed state of pluripotency, developmentally downstream of the naïve state[6] and unable to contribute substantially to blastocyst chimaeras. EpiSCs exhibit distinct growth factor, transcriptional and epigenetic regulation compared to ESCs. They self-renew when cultured in defined media containing FGF2 + ActivinA (F/A)[34,37,38], and lack significant expression of most functionally defined naïve pluripotency factors (Fig. S1f). EpiSC resetting proceeds over 6-8 days, much faster than somatic reprogramming, and entails primarily the activation and consolidation of the naïve identity[39–42]. In addition, EpiSC resetting does not require a complex reprogramming cocktail. The activation of Jak/Stat3 signalling[21,43,44] or forced expression of a single naïve TF factor[21,33,34] is sufficient to mediate reprogramming in combination with dual inhibition (2i) of the Erk pathway and glycogen synthase kinase-3 (GSK3)[45].

In this study, we undertook an iterative computational and experimental approach to test the hypothesis that a common network is sufficient to govern both naïve state maintenance and induction. Focusing on EpiSC resetting, we investigated whether naïve state induction follows an ordered sequence of network component activation. By refining our understanding of the network governing this process, we sought to delineate transcription factors crucial for the execution or the kinetics of EpiSC resetting, and identify synergistic

combinations. Finally, we extended the approach to investigate whether the same network architecture is operative in somatic cell reprogramming.

Results

Deriving a Set of Models Consistent with EpiSC Resetting

We previously studied the TF network controlling maintenance of naïve pluripotency[9] through a combined computational and experimental approach. Our methodology is based on the definition of relevant network components derived from functional studies in the literature, and the identification of 'possible' interactions between these components (Fig. 1a). Possible interactions are inferred based on gene expression correlation using the Pearson coefficient as a metric (Methods), and are used to define a set of alternative concrete Boolean network models, each with unique topology. We refer to this as an Abstract Boolean Network (ABN). We then define a set of experimental results, such as the effect of genetic perturbations, which serve as constraints to identify those models from the ABN that are relevant to the biological process of interest. The Reasoning Engine for Interaction Networks (RE:IN, www.research.microsoft.com/rein) is software based on automated formal reasoning, developed to synthesise only those concrete models that are provably consistent with the experimental constraints[9,15]. The set of consistent models is defined as a constrained Abstract Boolean Network (cABN), which is subsequently used to generate predictions of untested molecular and cellular behaviour. Our approach differs from typical modelling strategies in that we do not generate a single network model, but rather a set of models, which individually are consistent with known behaviours. We formulate predictions of untested behaviour only when all models agree, such that

predictions are consistent with the limits of current understanding. This is important because different network models can recapitulate the same experimental observations, and one should not be prioritised over another. Whenever predictions are falsified by new experimental results, it is possible to refine the cABN by incorporating the new findings as additional constraints (Fig. 1a). The refined cABN is then used to generate further predictions.

For the present study, we first refined the cABN describing maintenance of naïve pluripotency by adding further expression profiles generated using RNA-sequencing and RT-qPCR to the five datasets used previously[9] and by using an updated version of RE:IN[15] (Methods). We tested the refined naïve state maintenance cABN, defined by a Pearson coefficient threshold of 0.832 (Fig. 1b, S1a-c), against new gene perturbation experiments in mouse ESCs (Fig. S1d) and observed a significant increase in prediction accuracy over the previous version[9]. We therefore used the 0.832cABN as the starting point for analysis of EpiSC resetting.

We asked whether the naïve state maintenance cABN is consistent with experimental observations of EpiSC resetting. To this end, we exploited GOF18 EpiSCs, which are susceptible to resetting in 2i+LIF in the absence of transgenes[21]. In accordance with the Boolean modelling formalism, we discretised gene expression patterns of the network components for the initial (GOF18 EpiSC) and final (naïve state ESC) states, such that each gene is High/Low in each case (Fig. S1e and Methods). We defined a set of six new constraints based on known conditions under which EpiSC resetting can or cannot be achieved (Fig. 1c, Fig. S1f and Methods). For example, one constraint specifies that if a given

cell has none of the naïve pluripotency factors initially expressed, then 2i+LIF alone is not sufficient to induce the naïve state (Fig. 1c, top arrow). In contrast, resetting can be achieved if the initial state is equivalent to GOF18 EpiSCs, which express Oct4, Sox2 and Sall4 (Fig. 1c, third arrow from the top). We found that these additional constraints were satisfied by the naïve state maintenance cABN, which suggests that a single network may control both maintenance and induction of naïve pluripotency.

The number of concrete models in the 0.832 cABN is in the order of 10^5. As a control, we randomly generated 10,000 models with the same number of components and possible interactions. None of these models could satisfy the entire set of constraints. Indeed, if interactions with a Pearson correlation of at least 0.5 are chosen randomly, the probability of generating the 0.832 ABN is of the order 10^{-31}. This indicates that the data-driven approach facilitated identification of meaningful interactions between network components, and in practical terms substantially reduced the compute time for subsequent analyses. To test the requirement for each component in the cABN, we explored the consequence of deleting individual TFs from the network and constraints (Methods). Deleting 8 of the TFs made the initial constraints unsatisfiable. Only removal of Esrrb could be tolerated, but with substantially reduced number and accuracy of predictions. Therefore, the models are highly sensitive to all components of the cABN.

The dynamics of the concrete networks in the cABN were determined by a synchronous update scheme: from a given initial state, each and every component updates its state in response to its upstream regulators at each step (see Methods). Accordingly, we could examine the sequence of activation of each component along the trajectory towards the

naïve state. Fig. 1d shows the ordered activation of individual genes during EpiSC resetting in 2i+LIF from one concrete network in the 0.832 cABN. RE:IN can determine the number of regulation steps required for all models to reach the naïve state. This can be used as a metric to study the resetting process (Methods).

Prediction of Resetting Potency for Individual Network Components

Spontaneous GOF18 EpiSC resetting can be enhanced by expression of naïve network factors, such as Klf2[40,41,46], and such resetting events, measured by reporter activation, often possess faster activation kinetics than control[40]. The GOF18 EpiSC line contains a transgenic GFP reporter driven by the upstream regulatory region of Pou5f1 (Oct4). This transgene does not behave as endogenous Oct4. It is active in ESCs but only in a rare sub-population of EpiSCs. Therefore it serendipitously allows the live monitoring of EpiSC to ESC conversion[21]. We hypothesised that enhanced EpiSC resetting upon naïve factor expression may be due to accelerated network activation. We sought to test this computationally by determining the number of regulation steps required for *all* concrete models of the cABN to stabilise in the naïve state in 2i+LIF, with or without *Klf2* transgene expression. The 0.832 cABN predicted that forced expression of Klf2 in GOF18 EpiSCs results in the network stabilising in the naïve state in only 3 steps, compared with 5 steps for transgene-free control (Fig. S2a). Experimentally, we confirmed that transient Klf2 expression induced Oct4-GFP$^+$ colony formation earlier than empty vector control and led to higher colony number at day 10 of EpiSC resetting (Fig. S2b)[40]. Thereafter, we assumed that the number of Oct4-GFP$^+$ colonies obtained reflected EpiSC resetting dynamics and used this as an experimental output to compare with computational predictions.

We predicted the effect of forced expression of each network component using the 0.832 cABN (Fig. 1e). The predictions indicated that expression of all factors except Tbx3 and Sox2 would lead to stabilisation in the naïve state in fewer steps than control, indicating that most network components could enhance EpiSC resetting. For example, when Esrrb is introduced, all concrete models predicted full activation of the naïve network by step 2, compared to 5 steps for control.

To test these predictions experimentally, we generated expression constructs for each factor by cloning the cDNA into an identical vector backbone, and transiently transfected GOF18 EpiSCs one day prior to initiating resetting in 2i+LIF. We measured the relative efficiency between different components by the fold increase of Oct4-GFP^{+} colonies formed at day 7 over empty vector control (Fig. 1f, S2c). While some factors, such as Sall4 and Oct4, had no significant effect over control, others, notably Esrrb, Klf2, and Klf4, showed a robust enhancement. The computational predictions showed a similar trend to the experimental results, with seven out of eleven cases correctly predicted (Fig. 1e, S2d). Predictions for Tbx3, Stat3 and Oct4 transgene expression were incorrect. Most strikingly, Sall4 was predicted to be one of the most efficient factors, but was found to be the least efficient experimentally.

The iterative nature of our approach (Fig. 1a) allows the refinement of the cABN in the light of new experimental results that are predicted incorrectly. We encoded the experimental

observation that Sall4 expression was no more efficient than control as an additional constraint (Methods). Satisfying the new constraint together with the original set required increasing the number of possible interactions by lowering the Pearson coefficient threshold (Fig. 1g). The new threshold, 0.782 is the highest to define a cABN that satisfies the updated experimental constraints. We then generated a new set of predictions for single factor forced expression. In each case, we observed a range of steps for which some concrete models predict stabilisation in the naïve state, while others do not (Fig. 1h, light green). However, predictions can only be formulated when all concrete models are in agreement (Fig. 1h, dark green). Forced expression of Esrrb, Klf4, Gbx2, Klf2 or Tfcp2l1 were predicted to be more efficient than control, in agreement with the experimental results in Fig. 1f (see also Fig. S2d).

For forced expression of Nanog, Tbx3, Stat3, and Sox2, overlap of the light green regions with control prevented definitive predictions. To resolve this uncertainty, we formally tested *in silico* whether expressing a given factor would be more efficient than control for every concrete model. This resulted in the correct predictions that Nanog was always at least, or more efficient than control, while Stat3, Sox2 and Oct4 were not (Fig. S2d). The strategy did not generate a prediction for Tbx3 because some models display different kinetics. Note that the lack of effect of forced expression of Sall4 has been imposed as a constraint in the refined cABN, and is no longer considered to be a prediction.

We extended the test to perform a pairwise comparison of all genes so as to delineate the relative efficiency of individual factors (Fig. S2e). Predictions could be formulated for 42 out of 66 possible comparisons. Of these, 26 were supported experimentally, while 10 were

incorrect. For the remaining 6, the experimental results showed a trend in agreement with the predictions, although without reaching statistical significance due to variability in the naïve colony number between independent experiments. Fig. S2f summarises all significant pairwise comparisons with experimental support.

Delineating the Sequence of Network Activation

The 0.782 cABN accurately predicted the effect of forced expression of naïve components on EpiSC resetting, which suggests that resetting is not a random process. We therefore asked if resetting occurs via a precise sequence of gene activation, and whether this could also be identified using the cABN. Fig. 1d illustrates the dynamics of how one example concrete model stabilises in the naïve state. We investigated whether a defined sequence of gene activation was common to all concrete models, or whether individual models transition through unique trajectories. We focussed on those genes expressed at low levels in GOF18 EpiSCs, to enable unequivocal detection of activation over time in population-based measurements.

To predict the sequence of gene activation during EpiSC resetting, we examined the number of regulation steps required for each gene to be permanently activated in 2i+LIF without transgene expression (Fig. 2a). For Stat3, Tfcp2l1, Gbx2 and Esrrb, all models were in agreement, predicting that Stat3 and Tfcp2l1 were the first to be activated, at steps 1 and 2 respectively, while Gbx2, Klf4 and Esrrb were activated last, at steps 6 and 7. The wide range of step values for permanent Tbx3 activation predicted by different models within the cABN (Fig. 2a, light blue region) prevented a definitive prediction.

To test these predictions, we measured the expression of each gene over the EpiSC resetting time course in 2i+LIF for up to 4 days (Fig. 2b, c). We defined gene activation to be an up-regulated expression level that is statistically significant over EpiSCs. As predicted, Stat3 was significantly induced as early as 2 hours after 2i+LIF induction, Tfcp2l1 after 8 hours, while Klf4, Esrrb and Tbx3 only became detectable between 48 and 96 hours. In contrast to the predictions, Klf2 was significantly increased after only 1 hour of 2i+LIF treatment.

Tfcp2l1 and Esrrb are direct targets of the LIF/Stat3 and CH/Tcf3 axes[42,46–48]. However, even though CH and LIF were applied simultaneously to initiate resetting, Tfcp2l1 and Esrrb displayed distinct activation kinetics. We hypothesised that the local regulation topology of these two components may affect the timing of their activation. We therefore examined all immediate upstream regulators of Tfcp2l1 and Esrrb, and the logical update rules that define the conditions under which each component becomes active (Fig. 2d). Tfcp2l1 had six upstream activators, of which Stat3 and Esrrb were definite, and one inhibitor, Tcf3. Esrrb had three definite activators, Sall4, Nanog and Tfcp2l1, as well as a definite and an optional inhibitor. The computational methodology defines a set of 9 alternative update rules, referred to as regulation conditions, that span the possible scenarios under which a target can be activated. In the same manner in which some possible interactions were found to be required or disallowed when experimental constraints were applied to the ABN, certain regulations conditions were also found to be used or unused in order to satisfy the constraints. We compared the subset of regulation conditions assigned to Tfcp2l1 and Esrrb across all models, and one key difference emerged. While Tfcp2l1 required only one of its potential activators (Stat3, Esrrb, Tbx3, Gbx2, Klf2 or Klf4) to activate expression, Esrrb required the presence of all activators (Nanog, Tfcp2l1, Sall4) (Fig. 2d). Since Stat3 was

activated after 1 hour in response to 2i+LIF, early activation of Tfcp2l1 could therefore be attributed to Stat3. Esrrb would necessarily only be activated after activation of Tfcp2l1. This local topology analysis therefore provides a network explanation accounting for the rapid activation of Tfcp2l1 (8 hours, Fig. 2b) and the delayed activation of Esrrb (48 hours).

Combinations of Factors Can Enhance EpiSC Resetting

Earlier studies have shown that forced expression of a combination of factors can synergistically enhance resetting efficiency[40,44,46]. Our computational approach enabled us to investigate the effect of factor combinations in a systematic manner. We focused on those factors found to be potent inducers when expressed individually: Klf4, Klf2, Esrrb, Tbx3 and Tfcp2l1 (Fig. 1f). Six out of seven combinations were predicted to reduce the number of regulation steps required to induce and stabilise the naïve state (Fig. 3a, left). In the case of Esrrb/Tfcp2l1 dual expression, no enhancement beyond single factors was predicted.

We tested these combinations experimentally by transient transfection of the factors singly or combined. The number of reset Oct4-GFP^{+} colonies was scored at day 7 and resetting efficiency was calculated based on fold increase over empty vector control. The resetting efficiency of dual factor transfection was compared to individual factors alone to determine the combinatorial effect. Six out of seven experimental results were consistent with computational predictions (Fig. 3a, right). Five combinations (Esrrb/Klf2, Esrrb/Klf4, Esrrb/Tbx3, Klf4/Tbx3, Klf2/Tbx3) yielded synergistic enhancement, while two combinations (Esrrb/Tfcp2l1 and Klf2/Klf4) showed no greater effect than the single factors (Fig. 3a, right,

3b). These results demonstrate that the logic encoded within our data constrained set of models is sufficient to predict synergistic or non-additive behaviour of factor combinations.

Since dual expression of Esrrb/Tbx3 and Esrrb/Klf4 dramatically enhanced EpiSC resetting (Fig. 3b, right), we utilised these combinations to explore resetting dynamics in detail. We generated *PiggyBac* vectors harbouring doxycycline (DOX) inducible Esrrb-T2A-Klf4-IRES-Venus and Esrrb-T2A-Tbx3-IRES-Venus constructs. We delivered the transgenes into GOF18 EpiSCs together with a separate rtTA construct (Fig. 3c). The presence of Venus^{+} cells upon DOX treatment confirmed induction of transgene expression. As a control, we used an empty vector carrying only the DOX responsive element and IRES-Venus. To assay resetting potency, we transferred EpiSCs to 2i+LIF in the absence or presence of DOX (0.2 µg/ml) for 48h, and continued resetting in 2i+LIF only for an additional 4 days before scoring Oct4-GFP^{+} colonies (Fig. 3d). Cells transfected with the empty vector with or without DOX, or with expression constructs in the absence of DOX, showed spontaneous resetting at low frequency, as expected (Fig. 3e, top). In contrast, both factor combinations in response to DOX yielded robust Oct4-GFP activation. There were too many GFP^{+} colonies to score accurately, therefore we quantified the GFP signal intensity of randomly selected fields (Fig. 3e, bottom). This analysis demonstrated that DOX induction led to a 9-16-fold increase in Oct4-GFP expression.

To examine EpiSC resetting kinetics functionally, we replated cells after 2, 4, 6, or 8 days (Fig. 3d) at clonal density and scored the number of emergent Alkaline Phosphatase (AP) positive colonies. In the absence of DOX, both the empty vector and dual expression

transfectants exhibited gradual accumulation of a few colonies. After induction with DOX, however, dual factor transfectants displayed rapid production of numerous AP^+ colonies, commencing as early as day 2 and peaking at day 6 (Fig. 3f).

To investigate whether the effect of these combined factors extended to other EpiSC resetting systems, we expressed these combinations in an independent EpiSC line, OEC2, which carries an Oct4-GFP transgene and the chimeric LIF receptor GY118[44]. Resetting does not occur in this cell line in 2i+LIF alone. Similar to GOF18 EpiSCs, we found robust induction of Oct4-GFP^+ colony formation with DOX treatment, and could observe resetting to the naïve state with only 24 hours of DOX induction (Fig. S3).

Delineating the Sequence of Network Activation under Dual Factor Expression

We next used the cABN to investigate the sequence of gene activation that occurs upon dual factor expression. Predictions were generated for the number of regulation steps required for each component to be permanently activated (Fig. 4a, b top, Fig. S4), and compared with experimental results (Fig. 4a, b bottom). To generate the experimental results, we measured network component expression of DOX-inducible GOF18 EpiSCs carrying the empty vector, Esrrb-T2A-Tbx3 or Esrrb-T2A-Klf4 constructs, and treated with 2i+LIF in the presence or absence of DOX.

Under DOX treatment, Esrrb-T2A-Tbx3 transfectants showed a more robust activation of endogenous Klf2 and Klf4 at day 4 relative to non-induced cells, consistent with the prediction that these genes should be activated earlier (Fig. 4a). Stat3 upregulation was not

341 accelerated, also as predicted. However, in the case of Tfcp2l1, we detected enhanced
342 activation that was not predicted. For Esrrb-T2A-Klf4 expression, we observed accelerated
343 activation of Klf2 and Tbx3 at day 4 compared to control, consistent with predictions (Fig.
344 4b). Again, we observed enhanced activation of Tfcp2l1 that was not predicted, while Stat3
345 showed no enhancement over control. Importantly, the sequence of gene activation was
346 consistent in OEC2 EpiSCs (Fig. S3f). Of note, the level of Klf2 activation relative to ESCs is
347 much lower in OEC2 (Fig. S3f) compared to GOF18 EpiSCs (Fig.4a,b).
348
349 EpiSC resetting is typically an inefficient and asynchronous process (Fig. S2b), limited by
350 both technical and biological variability. Consequently, analysis of population-based
351 measurements could mask the precise sequence of gene activation in productive resetting.
352 Since the inducible Esrrb-T2A-Klf4 expression system significantly enhanced EpiSC resetting,
353 this enabled us to capture gene activation kinetics at single cell resolution. Examining gene
354 expression of different components within the same cell along the EpiSC resetting trajectory
355 should allow reliable characterisation of the sequence of network activation. To achieve
356 this, we sorted individual cells after 2 and 4 days in 2i+LIF with DOX treatment (Fig. 4c left).
357 We conducted single cell gene expression profiling by RT-qPCR of Day 2 Venus/GFP Low and
358 High and Day 4 Venus/GFP High cells that were clonogenic in 2i+LIF upon replating (Fig. 4c,
359 right). As controls, we included established mouse RGd2 ESCs[49] and un-induced parental
360 EpiSCs. We profiled selected genes that were differentially expressed between naïve ESCs
361 and primed EpiSCs along with the core pluripotency factors, Oct4 and Sox2 (Fig. 4 d, e, Table
362 S1). Robust activation of naïve ESC associated genes was observed in Day 4 Venus/GFP High
363 cells. Some genes, such as Oct4 and Nr5a2, showed even higher expression than in ESCs (Fig.
364 4d), possibly due to perduring expression of Esrrb and Klf4. Oct4 and Sox2 were reduced in

365 many, but not all, Day 2 Low cells, but were robustly expressed in some Day 2 High and all
366 Day 4 High samples (Fig. 4e). EpiSC enriched genes that are also expressed at low levels in
367 naïve ESCs, such as Otx2, Utf1 and Pim2, were downregulated at day 2. However, some Day
368 4 High cells re-acquired expression of those genes which are associated with early transition
369 from naïve pluripotency[49,50]. In established reset clones, however, their expression levels
370 were similar to ESCs (Fig. S5a). Naïve pluripotency in such reset clones are confirmed
371 functionally by generation of multiple high grade live-born chimera (Fig. S5b). Overall, the
372 single cell transcriptional analysis further validated the robust, stable activation of the naïve
373 network after 4 days of Esrrb-T2A-Klf4 expression.
374

375 ## Clustering of Single Cell Gene Expression Profile Reveals an EpiSC Resetting Trajectory

376 We explored the sequence of gene activation at single cell resolution by examining the
377 proportion of cells displaying expression of individual genes at different stages of resetting
378 to test whether these data were consistent with predictions. For example, the cABN
379 predicted that Klf2 would always be active before Tbx3, from which it follows that
380 upregulation of Tbx3 should not occur in the absence of Klf2.
381

382 To test these predictions, we first discretised the data by k-means clustering (Methods), and
383 calculated the proportion of cells at each resetting stage exhibiting the four expression
384 patterns: Klf2/Tbx3 both Low; Klf2 High and Tbx3 Low; Klf2/Tbx3 both High; and Klf2 Low
385 and Tbx3 High (Fig. 5, top row). The majority of cells at Day 2 were Klf2/Tbx3 double
386 negative, while such cells were not found at Day 4, nor in ESCs. By Day 4, the majority of
387 cells were Klf2/Tbx3 double positive, as for ESCs. We observed subpopulations in which Klf2

388 was High and Tbx3 was Low, mostly at Day 2 with Day 2 High cells containing more than Day
389 2 Low cells, while a negligible fraction of cells was Tbx3 High, Klf2 Low. This is consistent
390 with the prediction that Klf2 precedes Tbx3 activation during resetting upon Esrrb-T2A-Klf4
391 expression. Even when all cells were considered together, irrespective of resetting stage,
392 only rare cells exist in the Klf2 Low and Tbx3 High expression state. Importantly, a similar
393 fraction of such cells was found in the ESC population, indicating that they most likely reflect
394 transcriptional fluctuation or heterogeneity in the naïve state. Similarly, the cABN accurately
395 predicted that Klf2 will be high before Gbx2 activation, and sustained expression of Sox2
396 precedes Tfcp2l1 activation (Fig. 5, middle and bottom panels). As an independent
397 approach, we performed hierarchical clustering using the SPADE algorithm to visualise the
398 kinetics of gene activation[51,52] (Fig. S5c, d). This analysis confirmed our observations and also
399 allowed us to place factors that are not in the naïve network on to the resetting activation
400 timescale. For example, Nr5a2, a known resetting enhancing factor[53], activates in a similar
401 pattern to Klf2.

402

403 ## Identifying Required Components for Naïve Network Activation

404 We next investigated whether loss of specific network factors would block naïve network
405 activation. We used the cABN to predict network components required for EpiSC resetting
406 by investigating whether the network could permanently stabilise in the naïve state in the
407 absence of each factor (Fig. 6a). The 0.782 cABN predicted that two factors, Esrrb and Gbx2,
408 are dispensable for EpiSC resetting, while the remaining factors are required. In the case of
409 Tbx3 no prediction could be formulated.

410

411 To test these predictions, we transfected GOF18 EpiSCs with siRNAs against individual
412 network factors. EpiSC resetting was initiated 24 hours post transfection by switching from
413 F/A to 2i+LIF and Oct4-GFP^{+} colonies were scored at day 6 (Fig. 6b). Experimental results
414 confirmed that Gbx2 is dispensable for resetting. Furthermore, the requirements for Oct4,
415 Sall4, Sox2, Stat3, and Klf2 were accurately predicted. Knockdown of Esrrb and Tbx3
416 reduced but did not abolish colony formation. Overall, 6 out of 9 predictions were
417 consistent with experimental results.

418

419 The experimental results revealed distinct resetting behaviour upon Klf2 or Klf4 depletion.
420 Both were predicted to be required, yet Klf4 knockdown did not eliminate colony formation,
421 while Klf2 was found to be essential (Fig. 6b). This experimental result was counterintuitive
422 as well as not predicted. Klf4 and Klf2 show at least partially redundant function in ESC self-
423 renewal[54], and both were potent resetting inducers when expressed in GOF18 EpiSCs (Fig.
424 1f). To confirm the result, we generated *Klf2* and *Klf4* knockout (KO) GOF18 EpiSCs by
425 deleting the largest coding exons using CRISPR/Cas9 (Fig. S6a, b). Resetting in 2i+LIF using
426 two independent KO EpiSC clones confirmed the knockdown results: *Klf4* KO EpiSCs
427 generated Oct4-GFP^{+} colonies as efficiently as wild type control, while *Klf2* KO EpiSCs yielded
428 no Oct-GFP^{+} colonies (Fig. 6c). This observation was further validated using an independent
429 EpiSC line in which resetting is driven by hyperactivation of Stat3 (Fig. S6c).

430

431 To investigate the specific consequence of Klf2 loss for network activation, we examined the
432 expression of network components over the resetting time course for up to 4 days (Fig. 6d).
433 WT and KO EpiSCs showed similar patterns of expression for Oct4, Sox2 and Sall4. For up to

8 hours of resetting, *Klf2* KO cells behaved similarly to WT. However, *Klf2* KO cells failed to elevate the expression of Nanog and Tfcp2l1 at later time points. Factors activated after 2 days of resetting, such as Esrrb, Klf4 and Tbx3, failed to be activated in *Klf2* KO cells. Taken together, these data suggest that in the absence of Klf2, EpiSCs can respond to 2i+LIF to initiate resetting, but this response is not sustained. Of note, EpiSC markers - Pou3f1, Otx2, Fgf5 - were sharply downregulated in both WT and KO cells (Fig. 6d, middle), suggesting that Klf2 is not involved in the dissolution of EpiSC identity. Furthermore, in both WT and *Klf2* KO EpiSC resetting we observed similar upregulation at the population level of lineage-specific genes, such as Sox1 and Pax6 (ectoderm), T/Bra (primitive streak), Flk1 (mesoderm) and Pdgfrα (endoderm) (Fig. 6d bottom). This suggests that Klf2 does not exert a lineage repression function during resetting. In addition, *Klf2* deletion in ESCs did not affect multi-lineage differentiation (Fig. S6d).

We next asked whether forced expression of individual network factors could compensate for the loss of Klf2. To this end, we transiently expressed all individual factors and found that only Klf2 and Klf4 could rescue the *Klf2* KO phenotype (Fig. 6e). These results indicate that Klf2 is specifically required for initiating resetting in EpiSCs. Rescue by forced expression of Klf4 suggests that the two factors are functionally equivalent and that differences in the activation kinetics of the two factors during resetting (Fig. 2b) underlie the requirement for Klf2 and dispensability of Klf4 (see also Discussion).

We picked and expanded individual *Klf2* KO reset clones obtained via transient Klf2 expression at day 7, and confirmed they were free of integration of *Klf2* transgene by genomic PCR (Fig. S6e) and lack of Klf2 expression (Fig. S6f). We quantified gene expression

458 for naïve network factors in these lines, and found that Oct4, Tbx3, Tfcp2l1 and Klf4 levels
459 were comparable to control, while Sall4, Gbx2, Sox2, Stat3 and Nanog were elevated (Fig.
460 S6f). Only in the case of Esrrb was gene expression lower in *Klf2* KO iPSCs than in control.
461 Despite these differences, *Klf2* KO naïve cells showed sustained self-renewal. Therefore Klf2
462 is dispensable for maintenance in 2i+LIF once naïve pluripotency has been attained,
463 consistent with previous reports for ESC propagation[55].
464
465 In light of the unexpected finding that Klf2 was specifically required for EpiSC resetting, we
466 investigated the relevance of other network components for resetting versus maintenance
467 of naïve pluripotency. Predictions were generated and tested by siRNA transfection in self-
468 renewing ESCs followed by clonal assay[9] (Table S3). Stat3 and Klf2 emerged as specifically
469 highly important for resetting. Depletion of Tbx3, Essrb, Nanog and Sall4 also reduced EpiSC
470 resetting frequency, and had little effect on naïve state maintenance (Fig. 6f). Klf4, Tfcp2l1
471 and Gbx2 appear individually dispensable for maintenance and resetting, while Oct4 and
472 Sox2 are essential to both (Fig. 6f). These results indicate that EpiSC resetting and naïve
473 state maintenance display different sensitivity to network components, and that such
474 differences are correctly identified by the cABN.
475
476 We investigated the specific requirement for Stat3 in EpiSC resetting. Gbx2, Klf4 and Tfcp2l1
477 are the direct downstream effectors of Stat3[12,56,57]. We first examined activation of these
478 TFs in the absence of LIF, or upon Stat3 knockdown. Induction of Tfcp2l1 and Gbx2 were
479 significantly reduced at 24h in both conditions (Fig. S7a). Later induction of Klf4 was also
480 reduced following Stat3 depletion (Fig. S7b). To examine the functional contribution of
481 these factors downstream of Stat3, we conducted knockdown and rescue experiments.

Depletion of Tfcp2l1, Gbx2 or Klf4 either individually or in dual combinations does not inhibit GOF18 EpiSC resetting (Fig. 6a, g). However, combined loss of all three factors significantly reduced resetting efficiency (Fig. 6g) to levels comparable to Stat3 knockdown. In contrast, forced expression of individual factors rescued the effect of Stat3 knockdown (Figs. 6h, S7c). Taken together, we conclude that Tfcp2l1, Gbx2 and Klf4 are individually dispensable, but in combination they mediate the effect of LIF/Stat3 signalling.

The dispensability of Klf4 and Tfcp2l1 and partial requirement for Esrrb were not correctly predicted by our models (Fig. 6a). By including new constraints for the effect of Klf4 and Tfcp2l1 knockdown, we could derive a cABN that was fully consistent with the siRNA resetting phenotypes. Fig. 6i shows the refined cABN, defined by a Pearson threshold of 0.717, and also highlights the kinetics of gene activation during EpiSC resetting alongside the potency of individual factors in accelerating the resetting dynamics. Interestingly, the rich set of behaviours we have explored could be explained by as few as 32 interactions between all network components in one “minimal” network topology (Fig. S6g). We characterised both required and disallowed interactions in the 0.717 cABN against CHIP-sequencing data generated from self-renewing mouse ESCs[58] and found that 90.91% were supported (Table S4). This suggests that a large fraction of the interactions may be direct.

A Single Biological Program Governs Maintenance and Induction of Naïve Pluripotency

Developmentally distant somatic cell types such as mouse embryonic fibroblasts (MEFs) can be reprogrammed to naïve pluripotency with naïve factor combinations[59]. We therefore asked whether MEF reprogramming could also be predicted with our cABN. We first

surveyed the literature for those factor combinations present in our network that have been used to reprogram MEFs. Without encoding any additional constraints, the 0.717 cABN accurately computed the capacity for successful production of iPSCs for 5 combinations from the literature[16,19,20,24,25,59] (Fig. 7a). In each case, we assume a starting state in which all components are inactive, save those factors in the reprogramming cocktail. We next investigated the effect of adding single factors to OSKM in a systematic manner by comparing the number of regulation steps required to stabilise in the naïve state in LIF (Fig. 7b). Experimentally, we conducted OSKM reprogramming of primary MEFs with a Nanog-GFP knock in reporter (TNGA)[60]. Reprogramming was induced by LIF addition in the presence of Vitamin C and Alk inhibitor[17], and Nanog-GFP^{+} colonies were scored at day 12 (Fig. 7b, right). The 0.717 cABN accurately predicted that the addition of Nanog, Tbx3 and Esrrb would enhance reprogramming efficiency in presence of LIF[21,5,24,25], while Sall4, Gbx2, Klf2 and Tfcp2l1 would have no additive effect.

We also explored the effect of 2i on somatic cell reprogramming. We conducted reprogramming as before, but from day 6, 2i was supplemented until day 12 when Nanog-GFP^{+} iPS colonies were scored. 2i addition enhanced MEF reprogramming compared to LIF alone (Fig. 7c). However, LIF is critical to OSKM-driven reprogramming irrespective of 2i (Fig S7d), in agreement with model predictions and previous observations[20]. In 2i+LIF, 3 out of 4 predictions of enhanced OSKM proved correct (Nanog, Tbx3 and Esrrb, but not Sall4) (Fig. 7c). Taken together, these results indicate that the 0.717 cABN is consistent with and predictive of the majority of behaviours in MEF reprogramming.

527

528 The 0.717 cABN could also predict the dynamics of gene activation by computing the
529 number of steps required for each component of the network to be stably activated.
530 Compared with gene expression measurements both at population and single-cell level from
531 two independent studies[16,17], the cABN correctly predicted that Tfcp2l1 and Sall4 are
532 activated before Nanog and Esrrb in MEF reprogramming (Fig. 7d, e). The predicted
533 sequential activation of gene pairs was validated by comparing the proportion of cells
534 expressing individual genes at different stages of MEF reprogramming[16] at single cell
535 resolution (Fig. 7e). Taken together, these analyses suggest that a common gene regulatory
536 program for naïve state maintenance governs reprogramming both from EpiSCs and somatic
537 cells.

538

539 To confirm the predictive capacity of our final set of models, and compare with previous
540 iterations, we used the 0.717 cABN to formulate predictions previously generated for both
541 naïve state maintenance[9] and EpiSC resetting (Table S3). In total, the 0.717 cABN was
542 constrained against 47 experimentally-observed behaviours, and generated a further 107
543 predictions consistent with experimental observations (Table S3). When compared to the
544 previous generations of cABNs - that described by Dunn et al.[9] and the 0.782 cABN (Fig. 1g,
545 Table S3) - we observed a progressive increase in overall predictive accuracy as we refined
546 the models against new data (Fig. 7f).

547

Discussion

In this study, we undertook an iterative computational and experimental approach to uncover the logic of resetting post-implantation derived EpiSCs to the naïve ESC state of pluripotency. The method exploited the power of automated reasoning to constrain a set of possible network models against existing experimental observations, and subsequently to use this set of models to formulate predictions of untested behaviour. Our results reveal that the biological program ruling maintenance of the naïve state also governs installation of naïve pluripotency both from primed EpiSCs, and from developmentally distant somatic cells. The program that we have progressively refined captures a complex and rich set of behaviours, and thereby encapsulates the robust nature of the naïve state captured in 2i+LIF as well as the fragility of resetting and its dependency of the availability of specific core factors. Furthermore, the program is highly predictive: of 136 tested predictions, 78.68% were supported by experiment. We conclude that maintenance and induction of naïve pluripotency are under the control of the same biological program, which responds dynamically to the initial cell state and signals provided.

Initially, we investigated how forced expression of individual network components influences EpiSC resetting. The cABN forecast correctly that only some factors - Klf2, Klf4, Esrrb and Tbx3 – strongly enhance EpiSC resetting, and furthermore that certain pairs of factors act synergistically. Co-expression of Esrrb with Klf4 or Tbx3 produced a highly efficient resetting context, which permitted us to dissect the sequence of gene activation at the single cell level. Significantly, we could identify TFs that can be compensated by other

components during self-renewal, but are more stringently required under the conditions of EpiSC resetting.

Klf2, but not Klf4, was unexpectedly identified as critical for resetting. Yet Klf2 becomes dispensable after the naïve network is established due to functional redundancy with Klf4. We conclude that EpiSC resetting is a conditional process that is highly dependent on the sequence of gene activation, whereas the naïve state maintenance circuitry is robust due to layers of redundancy that confer network resilience[61].

An often overlooked aspect of modelling is the insight to be gained from analysing incorrect predictions. The distinction between Klf2 and Klf4, which are both members of the Krüppel-like family of TFs and share high sequence homology in the DNA binding domain, was neither predicted nor intuitive. In both naïve state maintenance and somatic cell reprogramming, these genes have been shown to have largely redundant function[25,54,55]. Furthermore, expression of Klf2 and Klf4 has a similar and potent effect on EpiSC resetting. However, only Klf2 is required for transgene-free EpiSC resetting. This can be understood in the context of the network topology by examination of the kinetics of gene activation. Klf2 is upregulated within the first 2h of resetting, whereas Klf4 becomes stably expressed only after 48h. Thus, inactivation of Klf2 leaves the cell devoid of both Krüppel-like family TFs for the first 2 days. Associated with this, naïve markers normally activated subsequently are not induced and resetting does not proceed. Inactivation of Klf4, in contrast, can be compensated for by the presence of Klf2, which is activated early and maintained throughout. The functional redundancy between Klf2 and Klf4 is exemplified in the observation that *Klf2* KO cells can be reset by transient expression of either Klf2 or Klf4.

595

596 Like Klf2, Stat3 is also a factor specifically required for resetting, and the potent effect of the
597 LIF/Stat3 axis in resetting was previously reported[42,44,62]. Here we clarified the downstream
598 mediators of Stat3 and observed that three direct targets, Klf4, Tfcp2l1 and Gbx2,
599 cooperatively induce naïve pluripotency. Indeed, only their triple inactivation phenocopies
600 the loss of Stat3 in GOF18 EpiSCs, while single expression of each is sufficient to rescue Stat3
601 knockdown. We previously found that Tfcp2l1 is required for the resetting of OEC2 EpiSCs,
602 which do not convert spontaneously[56]. In such cells, LIF/Stat3 signalling results in the
603 activation of Tfcp2l1 but not of Klf4[56]. Moreover, Klf2 induction is attenuated compared to
604 GOF18 (Fig 4 and S3F). The lack of robust activation of Klf2 and Klf4 may explain the
605 dependency on Tfcp2l1 for OEC2 resetting. Notably, however, other findings, such as
606 Esrrb/Klf4 dual factor synergy and *Klf2* KO phenotype have been confirmed in OEC2 cells. It
607 is well-known that EpiSC lines vary in their properties, including efficiency of resetting[69,70].
608 This is consistent with the contingencies revealed by our models.

609

610 It is currently debated whether acquisition of naïve pluripotency is an ordered process,
611 following a precise sequence of events, or a stochastic system in which individual cells
612 follow different trajectories. Our results suggest that productive EpiSC resetting is not
613 stochastic, given that the biological program we have derived operates under a
614 deterministic update scheme and is consistent with 154 experimental observations
615 (considering constraints and predictions together). This may seem counterintuitive, given
616 that some EpiSCs fail to reset in the presence of transgenes (Fig. 4c) and activation of
617 somatic lineage markers can be detected (Fig. 6d). However, we hypothesise that EpiSC
618 resetting is deterministic subject to an initial activation threshold. Technical impedance,

619 such as variable transgene expression, and biological stochasticity, may render some cells
620 irresponsive or aberrantly responsive. Crucially however, once cells overcome the initial
621 activation threshold they follow a deterministic trajectory.

622

623 Our analyses identified two distinct kinetics of network gene activation (Fig. 2b, d). Factors
624 such as Stat3, Tfcp2l1 and Klf2 are rapidly upregulated in 2i+LIF, followed later by factors
625 such as Klf4 and Esrrb. These different kinetics of gene activation could be associated with
626 different roles in naïve network installation. Rapidly-activating factors are important to
627 initiate naïve network activation, consistent with the observation that Stat3 and Klf2 are
628 essential to resetting (Fig. 6a). Slow-activating factors such as Esrrb could play a
629 consolidating role in network installation. In line with this, Esrrb activation is a rate-limiting
630 step for resetting, and Esrrb is one of the most potent factors to induce the naïve state,
631 though non-essential (Fig 6i). We speculate that different modes of activation for genes with
632 different functions could be integral to the information-processing performed by a cell.
633 Understanding how regulation mode is coupled to biological function in a given process may
634 contribute insight into biological computation and in turn enable the artificial synthesis of
635 molecular logic to achieve desired cell behaviour.

636

637 Finally, we demonstrated that the network program derived from observations of naïve
638 state maintenance and EpiSC resetting has both explanatory and predictive power in
639 somatic reprogramming. This further suggests that the late phase of somatic
640 reprogramming is deterministic[16,17], but also highlights that a common network logic
641 governs acquisition of naïve pluripotency from different starting cell types.

642

643 Although arguably the mouse naïve pluripotency network is one of the most well-
644 characterised GRNs, we consider that our methodology could be applied to study other
645 networks with less complete knowledge. Given a reliable preliminary set of network
646 components and interactions, the methodology has the flexibility to incorporate or
647 eliminate constraints and regulators. Importantly, it can evaluate network behaviour against
648 experimental observations and guide network refinement towards higher predictive
649 accuracy, and reality.
650
651 In summary, our analyses point to a common biological program that governs naïve
652 pluripotency maintenance and induction. The power and utility of the combined
653 computational and experimental methodology is exemplified by predicting the sequence of
654 gene activation that occurs during EpiSC and somatic reprogramming, even at single cell
655 resolution, and pinpointing which factors affect resetting efficiency. This method enabled
656 the identification of pairs of TFs that dramatically accelerate resetting, yielding an overall
657 efficiency increase of up to 50-fold. The refined cABN provides a platform for revealing
658 principles of network dynamics underlying pluripotency transitions, including the
659 emergence and dissolution of naïve pluripotency in the embryo[7]. Moreover, a similar
660 iterative methodology using the RE:IN tool[15] could be applied to study direct lineage
661 reprogramming[64–66]. We further envisage that our approach should be applicable to derive
662 an understanding of network architecture and dynamics underpinning other cell fate
663 transitions, given an experimentally derived initial set of definite and possible interactions.

Author Contributions

S-J.D. carried out the computational modelling. M.A.L., E.C. and G.M. carried out the experiments. S-J.D., M.A.L. and G.M. analysed computational predictions and experimental data. S-J.D., M.A.L., G.M., and A.S. designed the study and wrote the paper. A.S. and G.M. supervised the study.

Acknowledgements

We thank members of the Smith and Martello laboratories, and Boyan Yordanov and Christoph Wintersteiger from Microsoft Research for advice and discussion. We are grateful to Jose Silva, Sirio Dupont, Michelangelo Cordenonsi and Marco Montagner for critical reading of the manuscript. We thank Ge Guo for providing naïve factor constructs, Kosuke Yusa for OSKM reprogramming *piggybac* construct, Jose Silva for TNGA MEFs. We also thank Yosef Buganim for sharing the MEF reprogramming single cell RT-qPCR data. Sarah Gharbi and Anzy Miller for their assistance with the OpenArray system. We thank Andy Riddell for assistance for FACs sorting. S-J.D. is supported by Microsoft Research. G.M.'s laboratory is supported by grants from Giovanni Armenise-Harvard Foundation and Telethon Foundation (TCP13013). A.S. and M.A.L. are funded by the BBSRC. The Cambridge Stem Cell Institute receives core funding from the Wellcome Trust and Medical Research Council. M.A.L. was a Sir Henry Wellcome Postdoctoral fellow and received support from the University of Cambridge Institutional Strategic Support Fund. AS is a Medical Research Council professor.

References

1. Graf, T. & Enver, T. Forcing cells to change lineages. *Nature* **462,** 587–594 (2009).

2. Cahan, P. *et al.* CellNet: Network Biology Applied to Stem Cell Engineering. *Cell* **158,** 903–915 (2014).

3. Radley, A. H. *et al.* Assessment of engineered cells using CellNet and RNA-seq. *Nat. Protoc.* **12,** 1089–1102 (2017).

4. Rackham, O. J. L. *et al.* A predictive computational framework for direct reprogramming between human cell types. *Nat. Genet.* 1–8 (2016). doi:10.1038/ng.3487

5. Takahashi, K. & Yamanaka, S. Induction of pluripotent stem cells from mouse embryonic and adult fibroblast cultures by defined factors. *Cell* **126,** 663–76 (2006).

6. Nichols, J. & Smith, A. Naive and primed pluripotent states. *Cell Stem Cell* **4,** 487–92 (2009).

7. Boroviak, T. *et al.* Lineage-Specific Profiling Delineates the Emergence and Progression of Naive Pluripotency in Mammalian Embryogenesis. *Dev. Cell* **35,** 366–382 (2015).

8. Chen, X. *et al.* Integration of external signaling pathways with the core transcriptional network in embryonic stem cells. *Cell* **133,** 1106–17 (2008).

9. Dunn, S.-J., Martello, G., Yordanov, B., Emmott, S. & Smith, A. G. Defining an essential transcription factor program for naive pluripotency. *Science (80-.).* **344,** 1156–1160 (2014).

10. Herberg, M. & Roeder, I. Computational modelling of embryonic stem-cell fate control. *Development* **142,** 2250–60 (2015).

11. MacArthur, B. D. *et al.* Nanog-dependent feedback loops regulate murine embryonic stem cell heterogeneity. *Nat. Cell Biol.* **14,** 1139–47 (2012).

12. Niwa, H., Ogawa, K., Shimosato, D. & Adachi, K. A parallel circuit of LIF signalling pathways maintains pluripotency of mouse ES cells. *Nature* **460,** 118–22 (2009).

13. Rue, P. & Martinez Arias, A. Cell dynamics and gene expression control in tissue homeostasis and development. *Mol. Syst. Biol.* **11,** 792–792 (2015).

14. Yachie-Kinoshita, Ayako Onishi, K., Ostblom, J., Posfai, E., Rossant, J. & Zandstra, P. W. Modeling Signaling-Dependent Pluripotent Cell States With Boolean Logic Can Predict Cell Fate Transitions. *biorXiv* (2017). doi:10.1101/115683

15. Yordanov, B. *et al.* A method to identify and analyze biological programs through automated reasoning. *npj Syst. Biol. Appl.* **2,** 16010 (2016).

16. Buganim, Y. *et al.* Single-cell expression analyses during cellular reprogramming reveal an early stochastic and a late hierarchic phase. *Cell* **150,** 1209–22 (2012).

17. O'Malley, J. *et al.* High-resolution analysis with novel cell-surface markers identifies routes to iPS cells. *Nature* **499,** 88–91 (2013).

18. Stuart, H. T. *et al.* NANOG Amplifies STAT3 Activation and They Synergistically Induce the Naive Pluripotent Program. *Curr. Biol.* **24,** 340–346 (2014).

19. Tang, Y. *et al.* Jak/Stat3 signaling promotes somatic cell reprogramming by epigenetic regulation. *Stem Cells* **30,** 2645–2656 (2012).

20. Silva, J. *et al.* Promotion of Reprogramming to Ground State Pluripotency by Signal Inhibition. *PLoS Biol.* **6,** e253 (2008).

21. Han, D. W. *et al.* Epiblast Stem Cell Subpopulations Represent Mouse Embryos of Distinct Pregastrulation Stages. *Cell* **143,** 617–627 (2010).

22. Hanna, J. *et al.* Direct cell reprogramming is a stochastic process amenable to acceleration. *Nature* **462,** 595–601 (2009).

23. Sone, M. *et al.* Hybrid Cellular Metabolism Coordinated by Zic3 and Esrrb Synergistically Enhances Induction of Naive Pluripotency. *Cell Metab.* **25,** 1103–1117.e6 (2017).

24. Feng, B. *et al.* Reprogramming of fibroblasts into induced pluripotent stem cells with orphan nuclear receptor Esrrb. *Nat. Cell Biol.* **11,** 197–203 (2009).

25. Nakagawa, M. *et al.* Generation of induced pluripotent stem cells without Myc from mouse and human fibroblasts. *Nat. Biotechnol.* **26,** 101–106 (2007).

26. Mikkelsen, T. S. *et al.* Dissecting direct reprogramming through integrative genomic analysis. *Nature* **454,** 49–55 (2008).

27. Samavarchi-Tehrani, P. *et al.* Functional Genomics Reveals a BMP-Driven Mesenchymal-to-Epithelial Transition in the Initiation of Somatic Cell Reprogramming. *Cell Stem Cell* **7,** 64–77 (2010).

28. Tanabe, K., Nakamura, M., Narita, M., Takahashi, K. & Yamanaka, S. Maturation, not initiation, is the major roadblock during reprogramming toward pluripotency from human fibroblasts. *Proc. Natl. Acad. Sci.* **110,** 12172–12179 (2013).

29. Han, J. *et al.* Tbx3 improves the germ-line competency of induced pluripotent stem cells. *Nature* **463,** 1096–1100 (2010).

30. Golipour, A. *et al.* A Late Transition in Somatic Cell Reprogramming Requires Regulators Distinct from the Pluripotency Network. *Cell Stem Cell* **11,** 769–782 (2012).

31. Di Stefano, B. *et al.* C/EBPα poises B cells for rapid reprogramming into induced pluripotent stem cells. *Nature* **506,** 235–239 (2013).

32. Di Stefano, B. *et al.* C/EBPα creates elite cells for iPSC reprogramming by upregulating Klf4 and increasing the levels of Lsd1 and Brd4. *Nat. Cell Biol.* **18,** 371–381 (2016).

33. Silva, J. *et al.* Nanog is the gateway to the pluripotent ground state. *Cell* **138,** 722–37 (2009).

34. Guo, G. *et al.* Klf4 reverts developmentally programmed restriction of ground state pluripotency. *Development* **136,** 1063–1069 (2009).

35. Tsakiridis, A. *et al.* Distinct Wnt-driven primitive streak-like populations reflect in vivo lineage precursors. *Development* **141,** 1209–1221 (2014).

36. Kojima, Y. *et al.* The Transcriptional and Functional Properties of Mouse Epiblast Stem Cells Resemble the Anterior Primitive Streak. *Cell Stem Cell* **14,** 107–120 (2014).

37. Brons, I. G. M. *et al.* Derivation of pluripotent epiblast stem cells from mammalian embryos. *Nature* **448,** 191–195 (2007).

38. Tesar, P. J. *et al.* New cell lines from mouse epiblast share defining features with human embryonic stem cells. *Nature* **448,** 196–199 (2007).

39. Festuccia, N. *et al.* Esrrb Is a Direct Nanog Target Gene that Can Substitute for Nanog

764 Function in Pluripotent Cells. *Cell Stem Cell* **11,** 477–490 (2012).

765 40. Gillich, A. *et al.* Epiblast Stem Cell-Based System Reveals Reprogramming Synergy of Germline
766 Factors. *Cell Stem Cell* **10,** 425–439 (2012).

767 41. Hall, J. *et al.* Oct4 and LIF/Stat3 additively induce Krüppel factors to sustain embryonic stem
768 cell self-renewal. *Cell Stem Cell* **5,** 597–609 (2009).

769 42. Martello, G., Bertone, P. & Smith, A. Identification of the missing pluripotency mediator
770 downstream of leukaemia inhibitory factor. *EMBO J.* 1–14 (2013).
771 doi:10.1038/emboj.2013.177

772 43. Bernemann, C. *et al.* Distinct Developmental Ground States of Epiblast Stem Cell Lines
773 Determine Different Pluripotency Features. *Stem Cells* **29,** 1496–1503 (2011).

774 44. Yang, J. *et al.* Stat3 Activation Is Limiting for Reprogramming to Ground State Pluripotency.
775 *Cell Stem Cell* **7,** 319–328 (2010).

776 45. Ying, Q.-L. *et al.* The ground state of embryonic stem cell self-renewal. *Nature* **453,** 519–23
777 (2008).

778 46. Qiu, D. *et al.* Klf2 and Tfcp2l1, Two Wnt/β-Catenin Targets, Act Synergistically to Induce and
779 Maintain Naive Pluripotency. *Stem Cell Reports* **5,** 314–322 (2015).

780 47. Martello, G. *et al.* Esrrb is a pivotal target of the Gsk3/Tcf3 axis regulating embryonic stem
781 cell self-renewal. *Cell Stem Cell* **11,** 491–504 (2012).

782 48. Ye, S., Li, P., Tong, C. & Ying, Q.-L. Embryonic stem cell self-renewal pathways converge on
783 the transcription factor Tfcp2l1. *EMBO J.* **32,** 2548–2560 (2013).

784 49. Kalkan, T. *et al.* Tracking the embryonic stem cell transition from ground state pluripotency.
785 *Development* dev.142711 (2017). doi:10.1242/dev.142711

786 50. Acampora, D. *et al.* Loss of the Otx2-Binding Site in the Nanog Promoter Affects the Integrity
787 of Embryonic Stem Cell Subtypes and Specification of Inner Cell Mass-Derived Epiblast. *Cell*
788 *Rep.* **15,** 2651–2664 (2016).

789 51. Anchang, B. *et al.* Visualization and cellular hierarchy inference of single-cell data using
790 SPADE. *Nat. Protoc.* **11,** 1264–1279 (2016).

791 52. Qiu, P. *et al.* Extracting a cellular hierarchy from high-dimensional cytometry data with
792 SPADE. *Nat. Biotechnol.* **29,** 886–891 (2011).

793 53. Guo, G. & Smith, A. A genome-wide screen in EpiSCs identifies Nr5a nuclear receptors as
794 potent inducers of ground state pluripotency. *Development* **3192,** 3185–3192 (2010).

795 54. Jiang, J. *et al.* A core Klf circuitry regulates self-renewal of embryonic stem cells. *Nat. Cell Biol.*
796 **10,** 353–360 (2008).

797 55. Yeo, J.-C. *et al.* Klf2 Is an Essential Factor that Sustains Ground State Pluripotency. *Cell Stem*
798 *Cell* **14,** 864–872 (2014).

799 56. Martello, G., Bertone, P. & Smith, A. G. Identification of the missing pluripotency mediator
800 downstream of leukaemia inhibitory factor. *EMBO J.* 1–14 (2013).
801 doi:10.1038/emboj.2013.177

802 57. Tai, C.-I. & Ying, Q.-L. Gbx2, a LIF/Stat3 target, promotes reprogramming to and retention of
803 the pluripotent ground state. *J. Cell Sci.* **126,** 1093–8 (2013).

804 58. Sanchez-Castillo, M. *et al.* CODEX: a next-generation sequencing experiment database for the
805 haematopoietic and embryonic stem cell communities. *Nucleic Acids Res.* **43,** D1117–D1123
806 (2015).

807 59. Takahashi, K. & Yamanaka, S. Induction of pluripotent stem cells from mouse embryonic and
808 adult fibroblast cultures by defined factors. *Cell* **126,** 663–76 (2006).

809 60. Chambers, I. *et al.* Nanog safeguards pluripotency and mediates germline development.
810 *Nature* **450,** 1230–4 (2007).

811 61. Martello, G. & Smith, A. The Nature of Embryonic Stem Cells. *Annu. Rev. Cell Dev. Biol.* **30,**
812 647–675 (2014).

813 62. Carbognin, E., Betto, R. M., Soriano, M. E., Smith, A. G. & Martello, G. Stat3 promotes
814 mitochondrial transcription and oxidative respiration during maintenance and induction of
815 naive pluripotency. *EMBO J.* **35,** 618–634 (2016).

816 63. Chen, J. *et al.* H3K9 methylation is a barrier during somatic cell reprogramming into iPSCs.
817 *Nat. Genet.* **45,** 34–42 (2012).

818 64. Xie, H., Ye, M., Feng, R. & Graf, T. Stepwise Reprogramming of B Cells into Macrophages. *Cell*
819 **117,** 663–676 (2004).

820 65. Vierbuchen, T. *et al.* Direct conversion of fibroblasts to functional neurons by defined factors.
821 *Nature* **463,** 1035–1041 (2010).

822 66. Davis, R. L., Weintraub, H. & Lassar, A. B. Expression of a single transfected cDNA converts
823 fibroblasts to myoblasts. *Cell* **51,** 987–1000 (1987).

824 67. Yusa, K., Rad, R., Takeda, J. & Bradley, A. Generation of transgene-free induced pluripotent
825 mouse stem cells by the piggyBac transposon. *Nat. Methods* **6,** 363–369 (2009).

826 68. Yusa, K. *et al.* Targeted gene correction of α1-antitrypsin deficiency in induced pluripotent
827 stem cells. *Nature* **478,** 391–394 (2011).

828 69. Illich, D.J. *et al*. Distinct signaling Requirements for the establishment of ESC pluripotency in
829 late-stage EpiSCs. *Cell Rep.* **15**, 787-800 (2016).

830 70. Bernemann, C. *et al*. Distinct developmental ground states of epiblast stem cell lines
831 determine
832 different pluripotency features. *Stem Cells* **10**, 1496-1503 (2011).

Materials and Methods

Cell lines

All EpiSC lines in this work were cultured as described in [34] on fibronectin-coated plates in serum-free media N2B27 (DMEM/F12 and Neurobasal [both Life Technologies] in 1:1 ratio, with 0.1 mM 2-mercaptoethanol, 2 mM L-glutamine, 1:200 N2 [Life Technologies], and 1:100 B27 [Life Technologies]) supplemented with FGF2 (12 ng/ml) and Activin (20 ng/ml) produced in house. GOF18 EpiSCs were described in [21] and generously provided by Hans Schöler. OEC2-Y118F (Oct4-GFP) EpiSCs are described in Yang et al (2010). TNGA MEFs were cultured as described in O'Malley et al (2013)[17].

Plasmid constructions

Individual core pluripotency network factors were either amplified from cDNA or cloned from existing expression plasmids into pENTR2B donor vector. Subsequently the transgenes were gateway cloned into the same destination vector containing PB-CAG-DEST-bghpA and pGK-Hygro selection cassette. The sizes of final expression constructs range from 8.5kb to 10.7kb.

To construct the T2A linked inducible overexpression plasmids, Esrrb and either Tbx3 or Klf4 were PCR amplified with part of the T2A sequence flanking the 3' or 5' of the gene respectively. Three-way ligation of both gene fragments together with pENTR2B vector resulted in the fusion of EsrrbT2ATbx3 or EsrrbT2AKlf4. Subsequently the fusion constructs were gateway cloned into the same final destination vector containing TRE-CMV and a Venus reporter. To generate co-expression cell lines, cells were co-transfected with a plasmid containing rtTA and a Neomycin selection cassette.

Transient overexpression of factors for EpiSC resetting

1.5µg of plasmid DNA was transfected with 3µl of Lipofectamine2000 to 1x105 EpiSCs in suspension in Fgf2/ActivinA (F/A) containing N2B27 medium with Rock inhibitor Y-27632 (Sigma, 1:1000) overnight in one well of the 12 well plate. The next day, medium was switched to 2i/LIF medium to initiate reprogramming. GFP positive colonies were scored at day 7 of reprogramming. When a combination of two factors were co-transfected, 0.75µg of plasmid DNA of each factor were used. For the control single factor transfections, 0.75 µg of plasmid DNA harbouring the indicated factor together with 0.75µg of empty vector plasmid were used.

Generation of KO EpiSCs with CRISPR/Cas9

The gRNA pair were chosen to delete the largest coding exons within Klf2 and Klf4 to ensure the complete loss of function. The gRNA design was conducted using online CRISPR gRNA design tool https://www.dna20.com/eCommerce/cas9/input. The chosen gRNAs were based on the minimal off-target scores. The gRNA containing plasmids were cloned by annealing the complementary oligos indicated in Table S7, and cloned into BbsI digested pX458 vector (Addgene). The constructs were sequence validated before transfection.

A pair of gRNA containing plasmids based on px458 designed with specific deletion were transfected using Lipofectamine2000 (Invitrogen). 500 ng of each plasmid were transfected with 3 ul Lipofectamine2000 to 2x105 EpiSCs in suspension in Activin/Fgf2/Xav containing N2B27 medium with Rock inhibitor Y-27632 (Sigma, 1:1000) overnight in one well of the 12 well plate. The next day, the media was refreshed with Activin/Fgf2/Xav/Rock inhibitor and 48 hours post transfection, 2,000 GFP high cells were sorted into 6 cells for colony formation. Individual colonies were picked and genotyping was conducted from extracted genomic DNA by primers indicated in Table S7 to identify clones with designed deletion. For Klf2 KO, deletion from both gRNAs resulted in genotyping PCR product to shift from 890 bp representing the wild type allele to 130 bp. For Klf4 KO, deletion from both gRNAs resulted in genotyping PCR product to shift from 840 bp representing the wild type allele to 100 bp. Only homozygous mutants were chosen for subsequent experiment.

siRNA knockdown for EpiSC resetting

Final concentration of 20nM siRNAs together with 0.5 µl of Dharmafect 1 (Dharmacon, T-2001-01) was transfected to 1x105 EpiSCs in suspension in Activin/Fgf2 containing N2B27 medium with Rock inhibitor Y-27632 (Sigma, 1:1000) overnight in one well of the 12 well plate. At least 2 siRNAs were used for each target gene knockdown and the catalogue number of all siRNAs are shown in Table S5. The next day, medium was switched to 2i/LIF medium to initiate reprogramming. GFP positive colonies were scored at day 7 of reprogramming.

siRNA knockdown for ESC maintenance

To test the effect of knock down of individual factors on maintenance of naïve pluripotency we transfected siRNA in mES cells and replated them after 48h at clonal density, as described in [9]. 5 Days after plating we scored the number of pluripotent colonies, relative to cell transfected with a control siRNA. At least 2 siRNAs were used for each target gene knockdown and the catalogue number of all siRNAs are shown in Table S5.

EpiSC resetting of DOX inducible factor combinations

Cells with the stably integrated piggyBac transposase (500ng), piggybac constructs harbouring the DOX inducible factor combinations (375ng) and rTtA construct (125ng) were plated in N2B27 medium containing F/A. The next day, medium was switched to 2i+LIF with or without DOX 0.2µg/ml to for 2 days to induce transgene expression. At day 2 medium was switched to 2i + LIF. Images were acquired at day 6 and clonal assays were performed at day 2-6-8. (See also Fig. 3d). For single cell qPCR analysis of resetting intermediates, cells were kept in 2i+LIF+DOX throughout the experiment for up to 4 days. Clonal assay was performed by replating 250 cells in a well of a 12 well plate in 2i+LIF without DOX.

MEF reprogramming

All MEF reprogramming experiments were conducted at P2. 2.5x105 TNGA MEF were transfected with 2.5 µg of OSKM piggybac construct[67], 2.5 µg of naïve factor piggybac construct or empty vector, together with 1.9 µg of HyPBase[68] using NEON transfection system (Thermofisher). Transfected cells were plated in MEF medium and the next day, one tenth of cells were replated into 1 well of a 6 well with MEF medium supplemented with LIF,

50µg/ml ascorbic acid and 500nM Alk inhibitor A83-01, as described in O'Malley et al (2013)[17]. The Nanog-GFP+ colonies were scored at day 12. For experiments with 2i addition, they were added to MEF reprogramming media from day 6 onwards.

Alkaline Phosphatase staining

For AP staining, cells were fixed with a citrate–acetone– formaldehyde solution and stained using the Alkaline Phosphatase kit (Sigma, cat. 86R-1KT). Plates were scanned using a Nikon Scanner and scored manually.

RNA extraction, reverse transcription and Real-time PCR

Total RNA was isolated using RNeasy kit (Qiagen) and DNase treatment was conducted either after RNA purification or during column purification. cDNA was transcribed from 0.5~1 ug RNA using SuperScriptIII (Invitrogen) and oligo-dT priming. Real-time PCR was performed using on StepOnePlus and QuantStudio machines (Applied Biosystems) with Fast Sybr green master mix (Applied Biosystems). Target gene primer sequences and probes used are listed in Tables S6. Expression levels were normalised to Actinβ or Gapdh. Technical replicates for at least two independent experiments were conducted. The results were shown as mean and standard deviation calculated by StepOnePlus software (Applied Biosystems).

Single cell gene expression profiling

OpenArrays were custom designed by ThermoFisher with the Taqman assay ID shown in Table S8. Single cells were directly deposited by Fluorescence Activated Cell Sorting into 9µl of a pre-amplification mixture (CellDirect One-Step qRT-PCR kit, 11753-500) which contains 0.05x of each TaqMan assay, 1x CellDirect reaction mix, 200 ng/µl SuperscriptIII/Platinum Taq, 100 ng/µl SUPERRase-In (ThermoFisher) in DNA suspension buffer (TEKnova). The reverse transcription and gene specific PCR amplification was carried out in a thermal cycler with the following condition: 50°C for 30min, 95°C for 2 min followed by 24 cycles of 95°C for 15 sec, 60°C for 4 min. cDNA was diluted 1:10 and only cells with at least two housekeeping genes amplified were chosen for whole panel gene expression profiling. The cDNA samples were loaded onto an OpenArray using OpenArray AccuFill system and the quantitative real-time PCR was run using Quantstudio 12K Flex System. For gene expression analysis, the average of five all housekeeping genes (Actβ, Gapdh, Tbp, Ppia, Atp5a1) were used for normalisation.

RNA-sequencing

RGd2 mouse ESCs were derived and expanded in 2i for 6 passages and subsequently have been cultured in defined conditions on gelatin coated plates for five passages in N2B27 basal medium supplemented with four combinations of cytokine LIF (20ng/ml), GSK3 inhibitor CHIR99021 (CH, 3µM) and MEK inhibitor PD0325901 (PD, 1µM): PD+CH, PD+LIF, CH+LIF, and PD+CH+LIF. The cells were passaged every 3 days at a density of 15,000 cells per cm^2 with medium refreshed daily.

Total RNA was isolated with RNeasy RNA purification. Ribo-zero rRNA depleted RNA was used to generate sequencing libraries for wild type and Ephemeron knockout cells in PD/LIF and 8 hr withdrawal from PDL from three independent cell lines. Single end sequencing was performed and the reads were mapped using NCBI38/mm10 with Ensembl version 75

annotations. RNA-seq reads were aligned to the reference genome using tophat2. Only uniquely mapped reads were used for further analysis. Gene counts from SAM files were obtained using htseq-count with mode intersection non-empty, -s reverse. Differential gene expression analysis was conducted using Bioconductor R package DESeq2 version 1.4.5. DESeq2 provides two P-values, a raw P-value and a Benjamini-Hochberg P-value (adjusted p value). An adjusted p-Value threshold of 0.05 was used to determine differential gene expression (95% of the results are not false discoveries, error rate 0.05 = 5%). The data is available at the NCBI Gene Expression Omnibus (accession number: GSE111694).

Identifying Possible Interactions

The initial 0.832 ABN was constructed from a set of *definite* interactions downstream of LIF, CH and PD, based on previous experimental studies that identified the direct targets of these signals [12,33,42,46,47], and a set of *possible* interactions derived from our RNA-Seq and RT-qPCR datasets as follows.

Seven Pearson coefficients were generated for each gene pair, one from each dataset, which quantify the correlation in gene expression under the action of different combinations of LIF, CH and PD. An interaction between two genes was defined to be possible and positive if at least one of these coefficients was above a given threshold, and the majority of the remaining coefficients were greater than zero. Similarly, an interaction between two genes was defined to be possible and negative if at least one of these coefficients was below the negative of a given threshold, and the majority of the remaining coefficients were less than zero. In cases where there are positive coefficients above the threshold as well as negative coefficients below the threshold, we let the majority rule. Given that correlations alone do not reveal which gene behaves as the regulator, possible interactions are defined to be bidirectional.

We identified the Pearson correlation threshold by constructing a set of experimental constraints (Fig. 1c and S1f, as described below). We then sought the maximum Pearson coefficient threshold that generated a set of possible interactions that could satisfy these expected behaviours, using the RE:IN software to test for satisfiability. In doing so, we minimised the number of possible interactions, and therefore the number of concrete models in the ABN.

Discretising Gene Expression Measurements and Encoding Experimental Observations

We discretised the gene expression profile of GOF18 EpiSCs (Fig. S1e) by setting a gene to High if its expression was at least 0.5 of its level in mouse ESCs in 2i+LIF. We therefore discretised the GOF18 EpiSC state to be such that Oct4, Sox2 and Sall4 were High, while the remaining TFs were Low. MEK/ERK and Tcf3 were also set to High in these cells, as they are cultured in F/A.

We added a set of experimental observations to our existing set of constraints concerning maintenance of naïve pluripotency[9], by discretising gene expression profiles for the following experimental behaviours, shown in Fig. S1f and summarised in Table S2:

Control: If none of the pluripotency factors are initially expressed, then 2i+LIF alone is insufficient to reach the naïve state, which is defined to be the gene expression state of mouse ESCs cultured in 2i+LIF[9].

EpiSC in 2i+LIF: Starting from the discretised gene expression profile of GOF18 EpiSCs, 2i+LIF is sufficient for these cells to reset and stabilise in the naïve state[21,42].

EpiSC in 2i only: 2i alone is insufficient to reset GOF18 EpiSCs, and so we constrain the networks by excluding trajectories that reach this state under 2i[42].

EpiSC in 2i with Tfcp2l1 expression: Forced expression of Tfcp2l1 is sufficient to reset GOF18 EpiSCs in 2i alone[42].

Nanog knockout EpiSCs in 2i+LIF: Knocking out Nanog prevents EpiSCs from reaching the naïve state in 2i+LIF[18].

Nanog knockout EpiSCs in LIF+CH: Nanog knockout EpiSCs in the presence of LIF+CH is sufficient to activate Oct4, Esrrb, Klf2, Tfcp2l1, Klf4 and Stat3[18].

Each constraint consists of an initial and final discrete gene expression pattern, which are defined at specific steps along the network trajectory. We allow 20 steps for each experiment trajectory to stabilise. The final state is either unreachable (indicated by a bar over the final time step in Fig. S1f), or stable (indicated by an asterisk). In the case where the full gene expression state cannot be defined (e.g. Tfcp2l1 forced expression in 2i) then we define the final state at two sequential steps to ensure that the key genes are sustained.

We encoded these constraints together with the ABN into the RE:IN tool[15]. The discrete gene expression profiles are imposed as initial and final states of trajectories that network models must satisfy. RE:IN synthesises only those concrete network models consistent with this set of expected behaviours, which comprise the cABN.

When investigating the gene activation kinetics of resetting, we included the observation that forced expression of Sall4 in GOF18 EpiSCs does not increase the efficiency of resetting to the naïve state (Fig. 1f). To ensure that this holds for all models, we encoded a new constraint that defined when Sall4 expression is imposed, an EpiSC will not reach the naïve state at an earlier step than the case in which it is not, regardless of the step at which the latter occurs. This is illustrated in the Table S2. Similarly, the constraint we added concerning Klf4 knockout in EpiSC resetting is described in the same file.

We explored the sensitivity of our approach to missing components by testing whether the above constraints are satisfiable if each component is removed individually. For all components save Esrrb, we found removing the component from the ABN prevents the constraints from being satisfied. This demonstrates that these components are absolutely required to generate the expected behaviour of ESCs and EpiSC reprogramming. Removal of Esrrb along with the 5 constraints concerning Esrrb knockdown or forced expression, yields a cABN that can satisfy the remaining constraints but cannot explain known Esrrb phenotypes and has low predictive power.

Network Dynamics

Each concrete network model in the ABN is considered as a state transition system, with a deterministic update scheme. Dynamic behaviour emerges from the update functions that are applied to each component, which are logical functions that define how the gene updates its state in response to its regulators. Often such update functions are defined according to the named regulators of a given target, but given that we have an ABN, the regulators of a target can vary between concrete models. We therefore defined a set of twenty update functions that are not dependent on named regulators [15], which reason about whether some, all or none of a targets activators/repressors are present. In this present study, we consider a subset of these conditions (regulation conditions 0-8 as described in [15]), which assume that a gene requires at least one activator in order to be expressed. In a concrete model, each component is assigned one of these regulation conditions to ensure that the constraints are met.

Required and Disallowed Interactions

We characterise the cABN by identifying which of the possible interactions are common to all concrete networks – required interactions – and which are never present – disallowed interactions. A simple algorithm is implemented that first identifies a single concrete network consistent with the experimental observations. Each of the possible interactions that are instantiated as present in this example solution are subsequently removed individually from the ABN, and RE:IN identifies whether the constraints are satisfiable in the absence of the interaction. If the constraints are unsatisfiable when a given possible interaction is removed, then it must be the case that it is present in every concrete network that satisfies the constraints. Conversely, we examine all interactions not present in the example solution that we initially found, testing whether the constraints are still satisfiable if these interactions are individually imposed as definite. If, once a possible interaction is switched to being definite and the constraints are no longer satisfiable, we conclude that that particular interaction can never be present in any concrete model solution. The remaining interactions – those which can be removed or imposed individually without preventing the constraints from being satisfied – remain as possible, and will be needed in some concrete models, but not all.

Formulating Model Predictions

Via RE:IN, our approach automatically synthesises the entire set of models consistent with the expected behaviour of the experimental system. When we formulate predictions of untested behaviour we interrogate the entire set of consistent models, and only if they all are in agreement is a prediction generated and tested. The behaviour of only a subset of models, which may not be fully representative, is never tested experimentally.

To generate predictions, hypotheses are encoded as additional constraints, and we test whether they are satisfiable together with the set of expected behaviours. Crucially, we also test the null hypothesis – that under the same conditions the expected behaviour cannot be obtained. If both are satisfiable independently, then it must be the case that some models satisfy the hypothesis, while others satisfy the null hypothesis. If all models satisfy the hypothesis, while the null is unsatisfiable, then a prediction can be formulated based on all

concrete models that the hypothesis is correct. If the null hypothesis is satisfiable, while the hypothesis itself is unsatisfiable, then a prediction can also be made, which is that the expected behaviour is never observed.

For example, to test whether GOF18 EpiSCs can reset to the naïve state under Gbx2 knockdown in 2i+LIF, we formulate a constraint with these initial and final states. We then also formulate and test the constraint that GOF18 EpiSCs do not reach the naïve state under Gbx2 knockout in 2i+LIF. In this particular example, we found that our hypothesis constraint was satisfiable, while the null hypothesis constraint was unsatisfiable. Therefore, all concrete models predict that GOF18 EpiSCs will reset in 2i+LIF with Gbx2 knockdown, which was subsequently found to be consistent with experimental evidence.

Identifying the Number of Regulation Steps to Reach the Naïve State

To determine how many regulation steps are required to stabilise in the naïve state, starting from the EpiSC state, we formulate hypotheses for each possible case, e.g. that it stabilises at step 2, at step 3, at step 4, etc. As described above, for each case we also test the null hypothesis. In this manner, we deduced whether some, all or none of the models allowed EpiSCs to stabilise in the naïve state at a given regulation step.

RE:IN allows the user to implement an asynchronous scheme, in which a single gene updates at each step, and the order in which genes update is chosen non-deterministically. Under this scheme, if RE:IN determines that the constraints are satisfiable, this only ensures that there exists at least one model and path that is consistent with each constraint. That is, it is possible that the genes could update in a different order and reach a different state from the same initial conditions. Formulating predictions for the number of steps for all models to stabilise in the naïve state under an asynchronous update scheme would require further assumptions to be made. Either a limit would have to be placed on the maximum number of sequential updates for a specific gene, or a restriction to ensure that all genes update within a certain number of steps. It would also be important to consider what is considered 'fair' in implementing asynchronous updates, to avoid unrealistic scenarios such as the same gene repeatedly updating and no others.

K-means clustering to discretise the single cell gene expression

We used k-means clustering with k=2 on the log10-transformed single cell gene expression data (Fig. 4d) in order to discretise gene expression into High/Low, for which we identified a unique discretisation threshold for each gene. Of note, the mean expression levels in the two clusters differ by several orders of magnitude.

SPADE analysis

We conducted a SPADE analysis using SPADEV3.0 [51], using the default settings. This was carried out on the log10-transformed single cell gene expression data (Fig. 4d).

Quantification and Statistical Analysis

We used the student's t test with $p<0.05$ to define statistical significance. The specific details of the test, number of the experiments (n), and the dispersion and precision

measurements (mean, median, standard errors and standard deviations) can be found in figure legends for Fig. 1f, S2 and 2B.

Data and Software Availability

The files used to generate the cABN will be made available at research.microsoft.com/rein, which also provides a tutorial for the tool, and FAQ. These have been made available to reviewers with this submission.

Supplemental Items

Fig. S1: (Related to Fig. 1) Deriving and constraining the 0.832 ABN.

Fig. S2: (Related to Fig. 1) Predicting the relative potency of single factor forced expression in enhancing resetting to the naïve state.

Fig. S3: (Related to Fig. 3) Investigating dual factor expression in OEC2-GY118 EpiSCs.

Fig. S4: (Related to Fig. 3 and Fig. 4a, b) A comparison of the resetting kinetics under empty vector control and dual factor expression, visualised on the 0.782 cABN.

Fig. S5: (Related to Figs. 4 and 5): Analysis of resetting time course using SPADE and clones generated by forced expression of Esrrb-T2A-Klf4 for 4 days.

Fig. S6: (Related to Fig. 6) Klf2 and Klf4 KO EpiSC generation and transgene free Klf2KO iPSCs.

Fig. S7: (Related to Fig. 7) Investigation of stat3 downstream effectors in EpiSC resetting (a-c, related to Fig 6), and LIF requirement in MEF reprogramming.

Table S1: (Related to Fig. 4) Single cell gene expression of ESC and EpiSC associated genes quantified by real time quantitative PCR.

Table S2: (Related to Fig. 6) The set of experimental constraints imposed on the 0.717 ABN.

Table S3: (Related to Fig. 6h) Comparison of predictions generated by 0.832, 0.782 and 0.717 cABN to the experimental observations.

Table S4: (Related to Fig. 6) Required and disallowed interactions in 0.717 cABN compared to the the CHIP-sequencing data.

Table S5: siRNAs used in this study.

Table S6: Real-time quantitative PCR primers and probes.

Table S7**:** DNA oligonucleotides used to generate gRNAs and genotype Klf2 and klf4 knockouts.

Table S8: Custom Taqman OpenArray real-time quantitative PCR IDs used for the single cell gene expression.

1154

1155

Figure 1

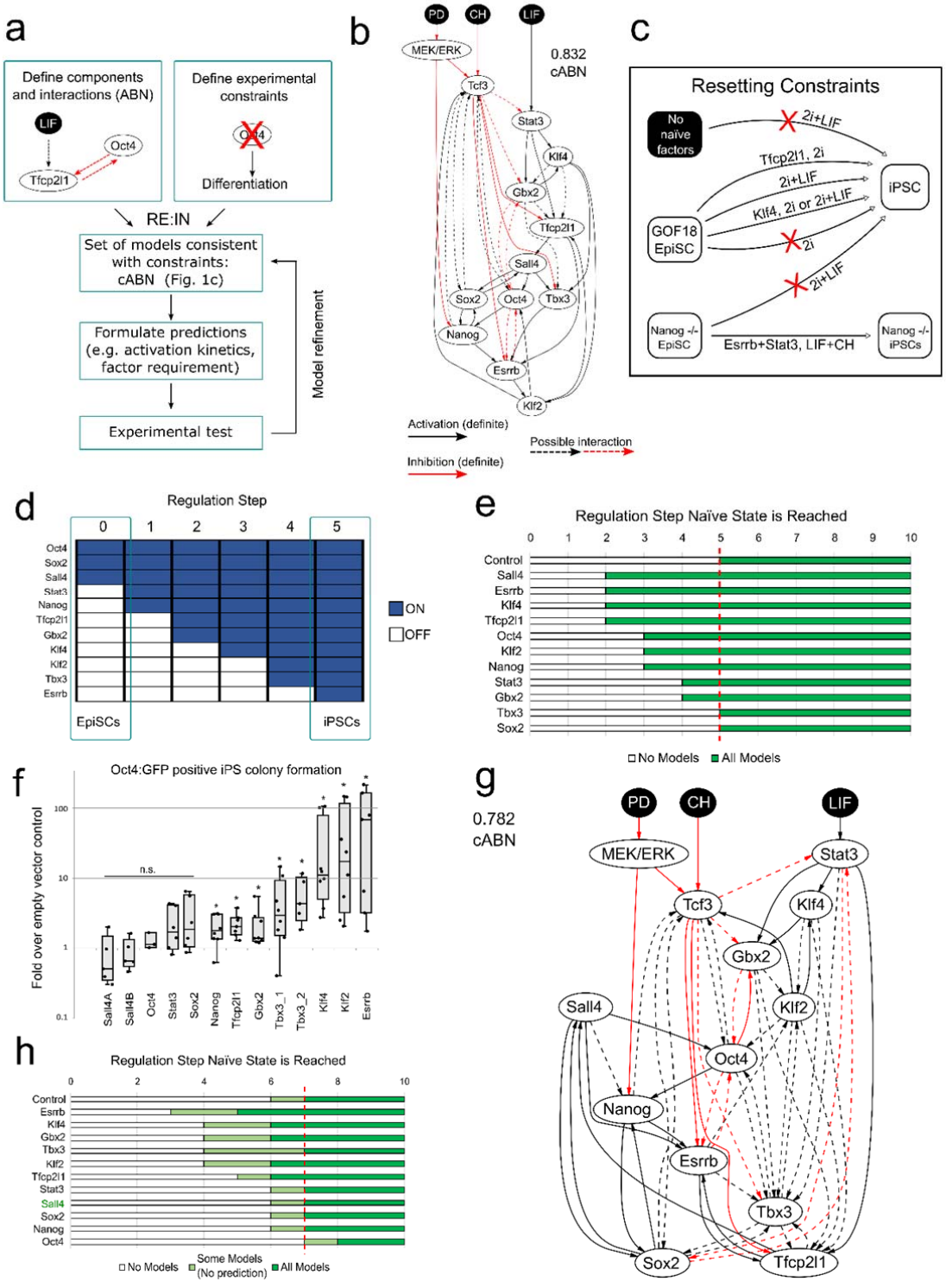

Figure 1: Network models consistent with naïve state maintenance predict the effect of TF forced expression in resetting from primed pluripotency. See also Fig. S1, S2. (a) Flow-chart describing the methodology. Network components were identified based on functional studies from the literature, and possible interactions between components defined based on pairwise gene expression correlation. A set of experimental results served as constraints. The software RE:IN synthesises all possible interaction networks consistent with the constraints, which is termed the cABN. The cABN is used to formulate predictions to be tested experimentally. If predictions are falsified, the cABN can be further refined by incorporating new findings as constraints. The refined cABN is used to generate further predictions. (b) cABN derived from a Pearson coefficient threshold of 0.832, consistent with constraints previously defined for ESC self-renewal (Dunn et al. 2014). Solid arrow, required interaction; dashed arrow, possible interaction; black arrow, activation; red arrow, inhibition. (c) Illustration of the EpiSC resetting constraints. See Fig S1f. (d) Example of the sequence of gene activation of naïve network components during EpiSC resetting, represented by regulation steps of the network trajectory. (e) Predicted number of regulation steps required for all models to stabilise in the naïve state under forced expression of single network component. Red dashed line indicates the number of steps required under empty vector control. (f) Fold increase of Oct4-GFP^{+} colony number under forced expression of individual factors over empty vector control. $n \geq 5$. Each dot indicates an independent experiment. Box-plots indicate 1st, 3rd quartile and median. *= $p<0.05$ Student's t-test; n.s.= not significant. (g) cABN derived from a Pearson coefficient threshold of 0.782. (h) Predictions from the 0.782 cABN. Light green regions indicate where some, but not all, concrete networks allow stable conversion to the naïve state. Sall4 indicated in green, as this was imposed as a constraint and therefore is not a model prediction.

Figure 2

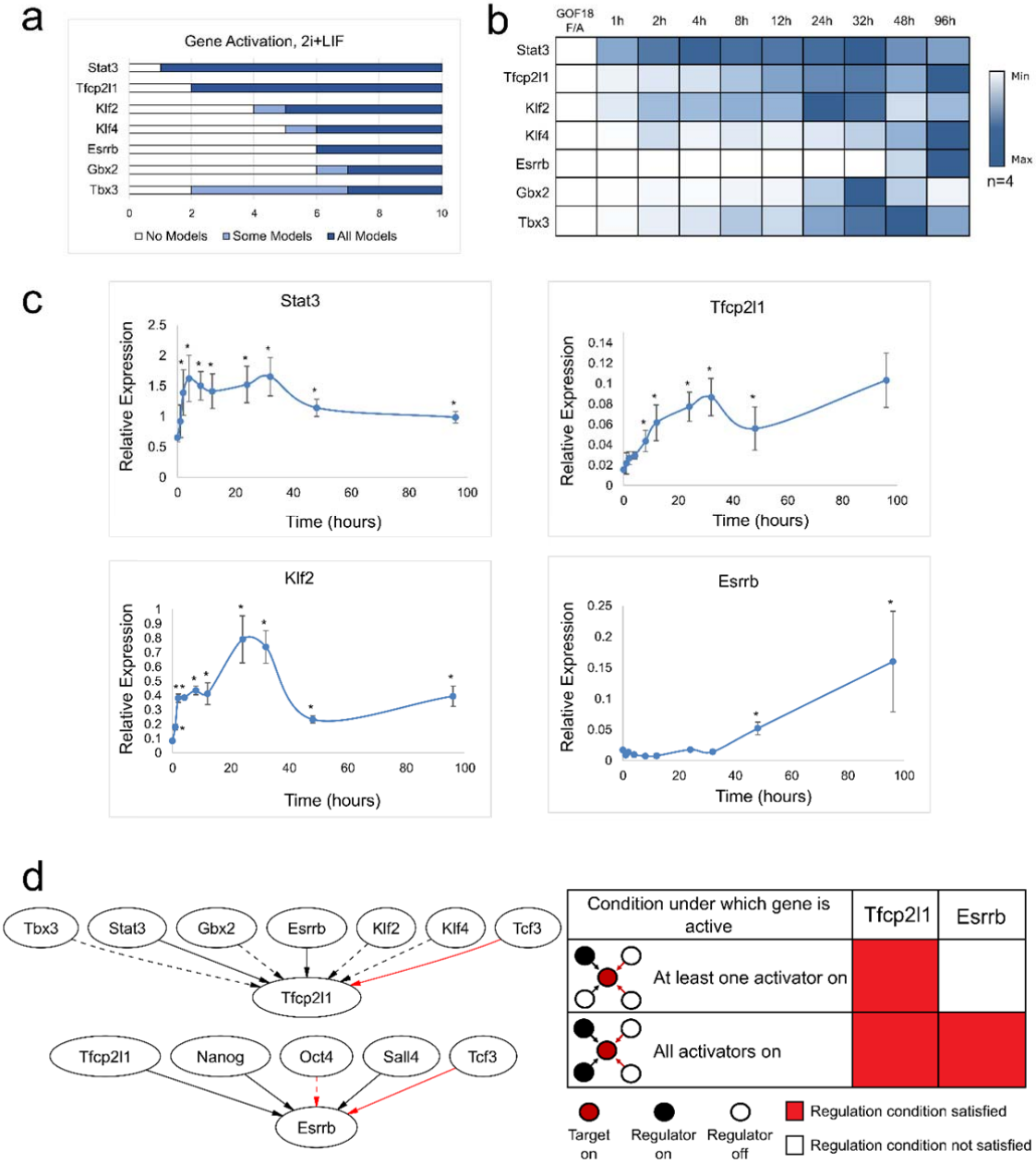

Figure 2: Models predict the sequence of gene activation of the naïve network. (a) Model predictions of the number of regulation steps required for permanent activation of gene expression of each network component. Light blue regions indicate where only some models predict the given gene has permanently activated. (b) A heatmap of the average gene expression normalised to β-actin over an EpiSC resetting time course in 2i+LIF. Each row is coloured according to the unique minimum and maximum for that gene. n=4. (c) Gene expression for Stat3, Klf2, Esrrb and Tfcp2l1 during EpiSC resetting relative to established mouse ESCs. Mean +/- SEM, n=4. *, Student's t-test, $p<0.05$. (d) Left: Local network topology for Tfcp2l1 and Esrrb. Right: Summary of regulation conditions required by Tfcp2l1 and Esrrb in the 0.782 cABN.

Figure 3

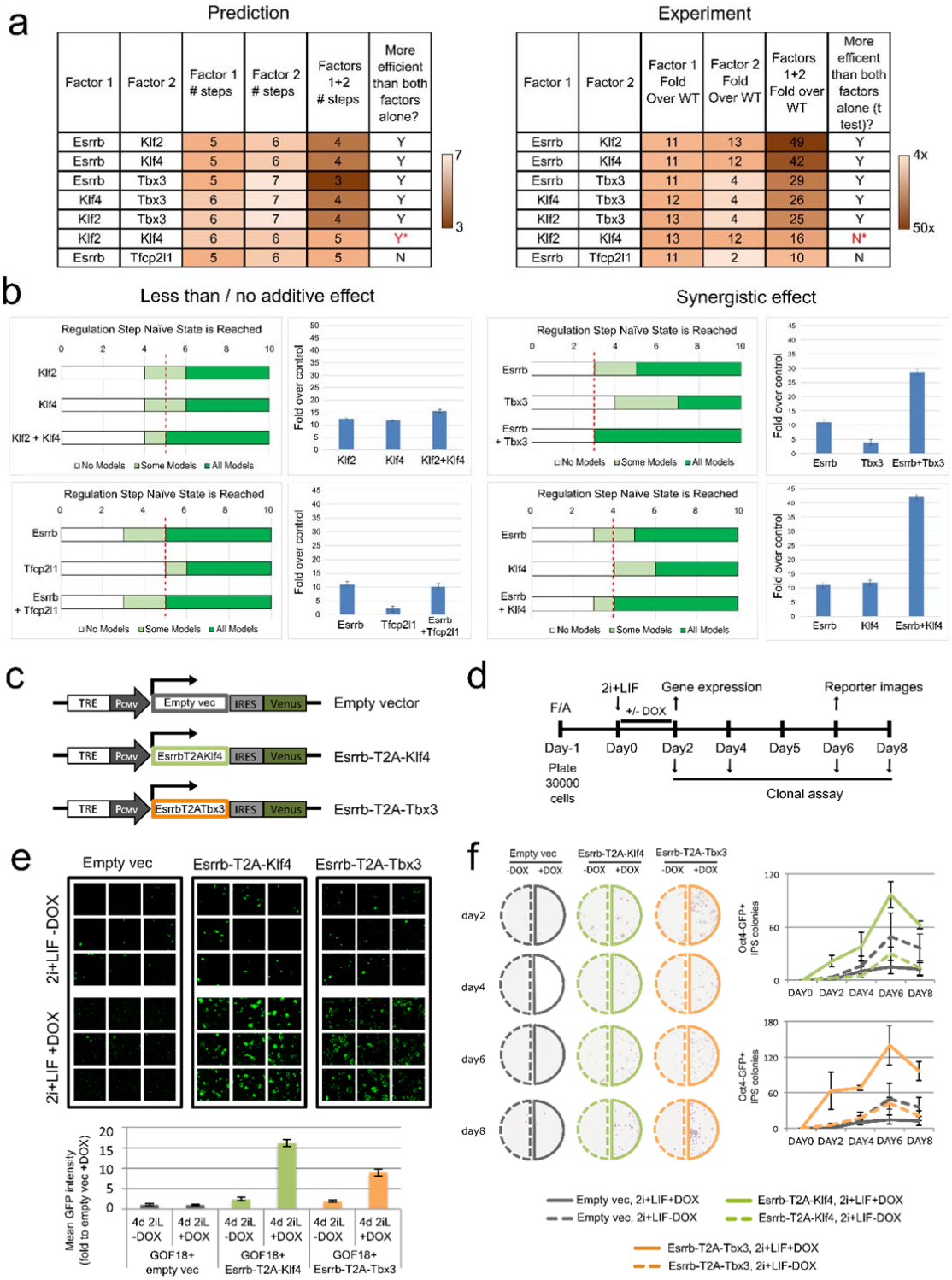

Figure 3: Combinations of potent factors enhance resetting by accelerating network activation. See also Fig. S4. (a) Left: Comparison of the number of steps required for all models to stabilise in the naïve state under single and dual factor expression. Right: Experimental results showing the fold increase in colony number over empty vector control, under single and dual factor expression. Y = Yes, N = No, * = incorrect prediction. (b) Predictions and experimental validation of examples of synergistic and non-additive factor combinations. Fold increase over empty vector control of Oct4-GFP^{+} colony numbers was measured experimentally. Mean +/- SD, n=2. (c) Cartoon for DOX inducible constructs used for dual factor expression. (d) Experimental scheme for functional characterisation of Esrrb-T2A-Klf4 or Esrrb-T2A-Tbx3 forced expression in EpiSC resetting. (e) Representative confocal images (top) and quantification (bottom) of Oct4-GFP reporter mean intensity (Top). The indicated cell lines were treated with DOX for the first 2 days and imaged at Day 6. Mean +/- SEM, n=2. (f) Representative alkaline phosphatase (AP) staining images (left) and quantification (right) of AP^{+} colonies after clonal replating, as described in panel D. Mean +/- SEM, n=3.

Figure 4

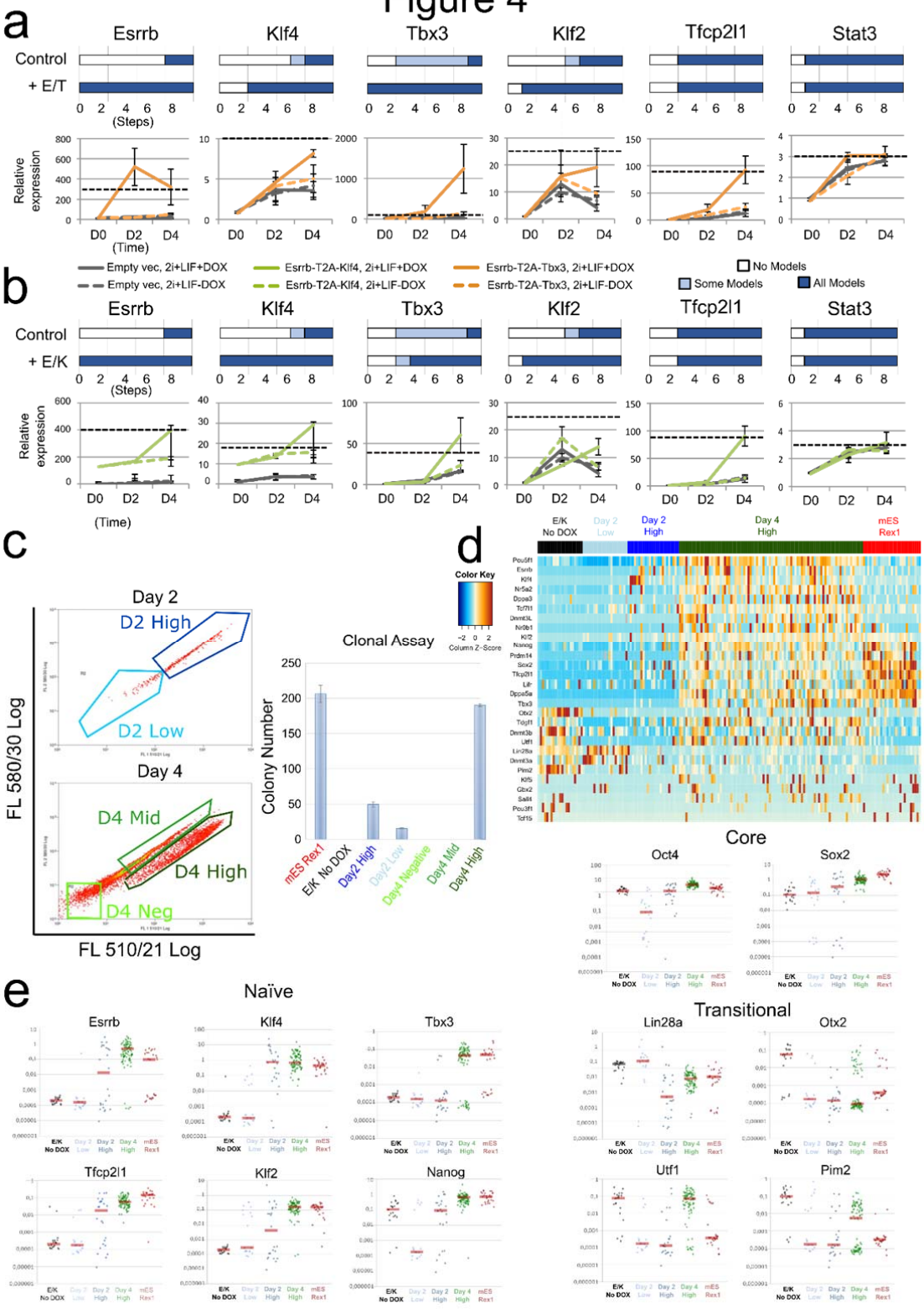

Figure 4: Co-expression of factors activated late in EpiSC resetting increases pluripotency marker expression and significantly reduces the resetting time scale. See also Fig. S3, S5, Table S1. (a) Top: Predictions of the number of regulation steps required for full activation of the indicated gene under control or dual expression of Esrrb and Tbx3 (+E/T). Bottom: Gene expression of EpiSCs harbouring empty vector (grey) or Esrrb/Tbx3 (orange), captured at D0 (F/A), D2 and D4 (as described in Fig. 3d). Dashed black line: expression levels in ESCs maintained in 2i+LIF. Data normalised to empty vector cultures in F/A. Gapdh serves as an internal control. Mean +/- SEM, n=3. (b) As for (a), comparison of control with dual expression of Esrrb and Klf4 (+E/K, green in bottom plot). (c) Left: Flow cytometry profiles of resetting progression of EpiSCs stably transfected with the Esrrb-T2A-Klf4 construct and cultured in 2i+LIF with DOX for 2 and 4 days, with indicated fractions of cells sorted for colony formation assay. Since the Venus reporter is under the control of a DOX responsive element, and the emission spectra of Venus and GFP fluorescence overlap, Oct4-GFP reporter expression could not be fully distinguished from Venus fluorescence. Right: number of AP^{+} colonies formed from 250 sorted cells from indicated fractions. (d) Heatmap of single-cell expression of major ESC and EpiSC markers in un-induced EpiSCs (black), established ESCs (Red) and Day 2 High/Low (dark and light blue) and Day 4 High cells (green). (e) Scatterplots of single-cell expression of pluripotency and transitional markers. Red bar, median gene expression.

Figure 5

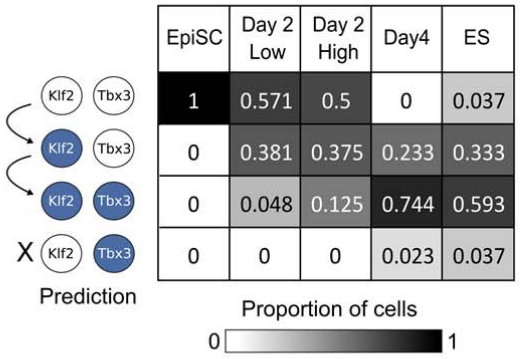

EpiSC	Day 2 Low	Day 2 High	Day4	ES
1	0.571	0.5	0	0.037
0	0.381	0.375	0.233	0.333
0	0.048	0.125	0.744	0.593
0	0	0	0.023	0.037

Proportion of cells

0 1

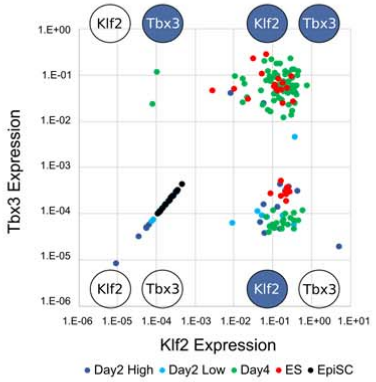

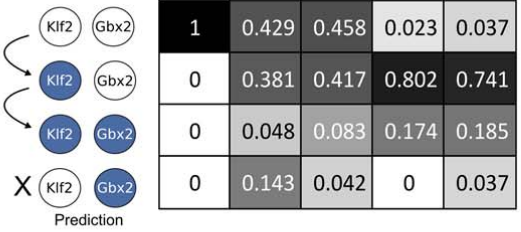

EpiSC	Day 2 Low	Day 2 High	Day4	ES
1	0.429	0.458	0.023	0.037
0	0.381	0.417	0.802	0.741
0	0.048	0.083	0.174	0.185
0	0.143	0.042	0	0.037

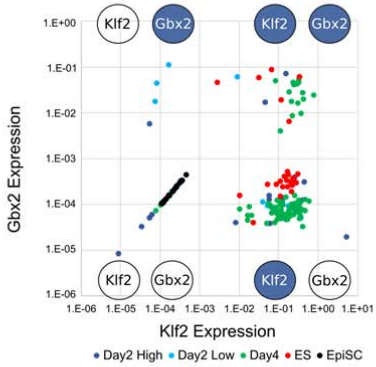

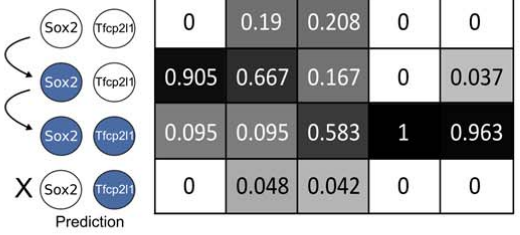

EpiSC	Day 2 Low	Day 2 High	Day4	ES
0	0.19	0.208	0	0
0.905	0.667	0.167	0	0.037
0.095	0.095	0.583	1	0.963
0	0.048	0.042	0	0

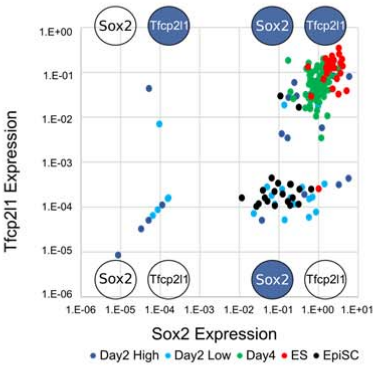

Figure 5: Single cell gene expression profiles recapitulate predicted sequence of gene activation. Left panels: predictions from the 0.782 cABN of the sequence of gene activation between gene pairs (white, OFF; blue, ON) along the resetting trajectory, compared to single cell gene expression measured by RT-qPCR. Each table summarises the percentage of single cells at the indicated stage of resetting (columns) that have the indicated expression state (rows). Right panels: Scatterplots showing single cell coordinates based on the expression of the gene pair.

Figure 6

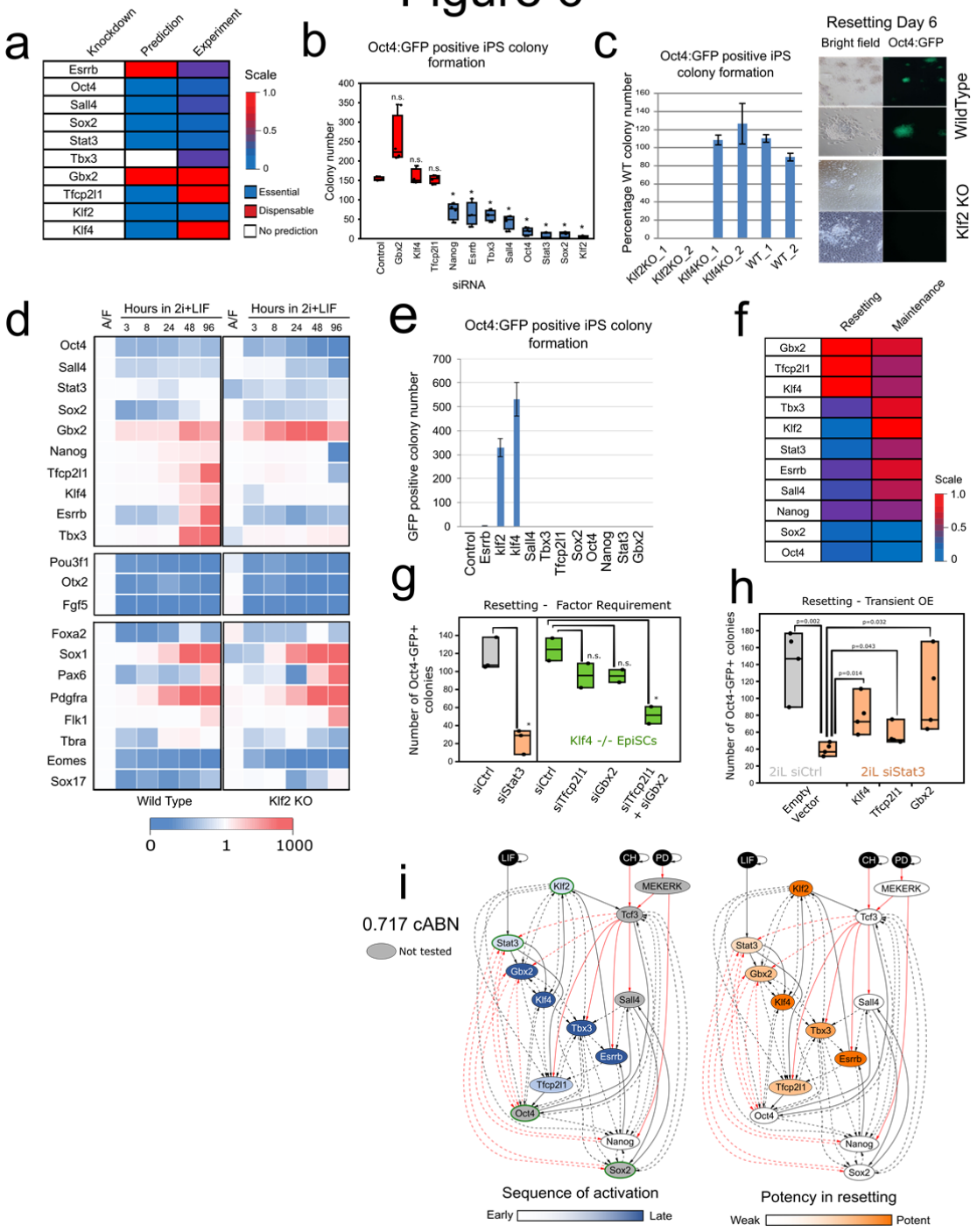

Figure 6: Klf2 and Stat3 are required factor for EpiSC resetting, but not for naïve state maintenance. See also Fig. S7, Tables S2-4. (a) Predictions from the 0.782 cABN of factors that are essential or dispensable for EpiSC resetting, compared against experiment results shown in b. (b) siRNA knockdown effects measured by Oct4-GFP^{+} colony formation. n=4; Each dot indicates an independent experiment. Box-plots indicate 1st, 3rd quartile and median. *= p<0.05 Student's t-test; n.s.= not significant.Student t-test, * p<0.05. n.s. not significant. (c) Left, resetting capacity of Klf2 and Klf4 KOs EpiSCs measured by Oct4-GFP^{+} colony formation. Right, representative fluorescent and bright field images of wild type and Klf2 KO EpiSC at day 6 of resetting in 2i+LIF. (d) Expression of naïve pluripotency, transition and somatic lineage markers in wild type and Klf2 KO EpiSCs during a resetting time course in 2i+LIF. Expression is normalised to wild-type EpiSCs in A/F. (e) Rescue of Klf2 KO EpiSC resetting by forced expression of individual network components. (f) Comparison between the effect of single factor knockdowns on ESC maintenance and EpiSC resetting using experimental results. (g) EpiSC resetting in 2i+LIF measured by Oct4-GFP^{+} colony formation after Stat3 siRNA in wild-type EpiSCs (left), or Klf4 KO EpiSCs transfected with Tfcp2l1 and Gbx2 siRNAs. n=2, Student's t-test, *: p<0.05. (h) EpiSC resetting in 2i+LIF measured by Oct4GFP^{+} colony formation of Stat3 knockdown EpiSCs transient transfected with Tfcp2l1, Gbx2 and Klf4. n=4: Student's t-test, p-value indicated on plot. See also Fig S7c. (i) The 0.717 cABN, used to illustrate the kinetics of EpiSC resetting. Left: Genes coloured according to the order of activation during resetting in 2i+LIF. Right: Genes coloured according to their potency in enhancing the efficiency of resetting. TFs with a green border are the common factors required for ESC self-renewal and EpiSC resetting. See also Fig S6g

Figure 7

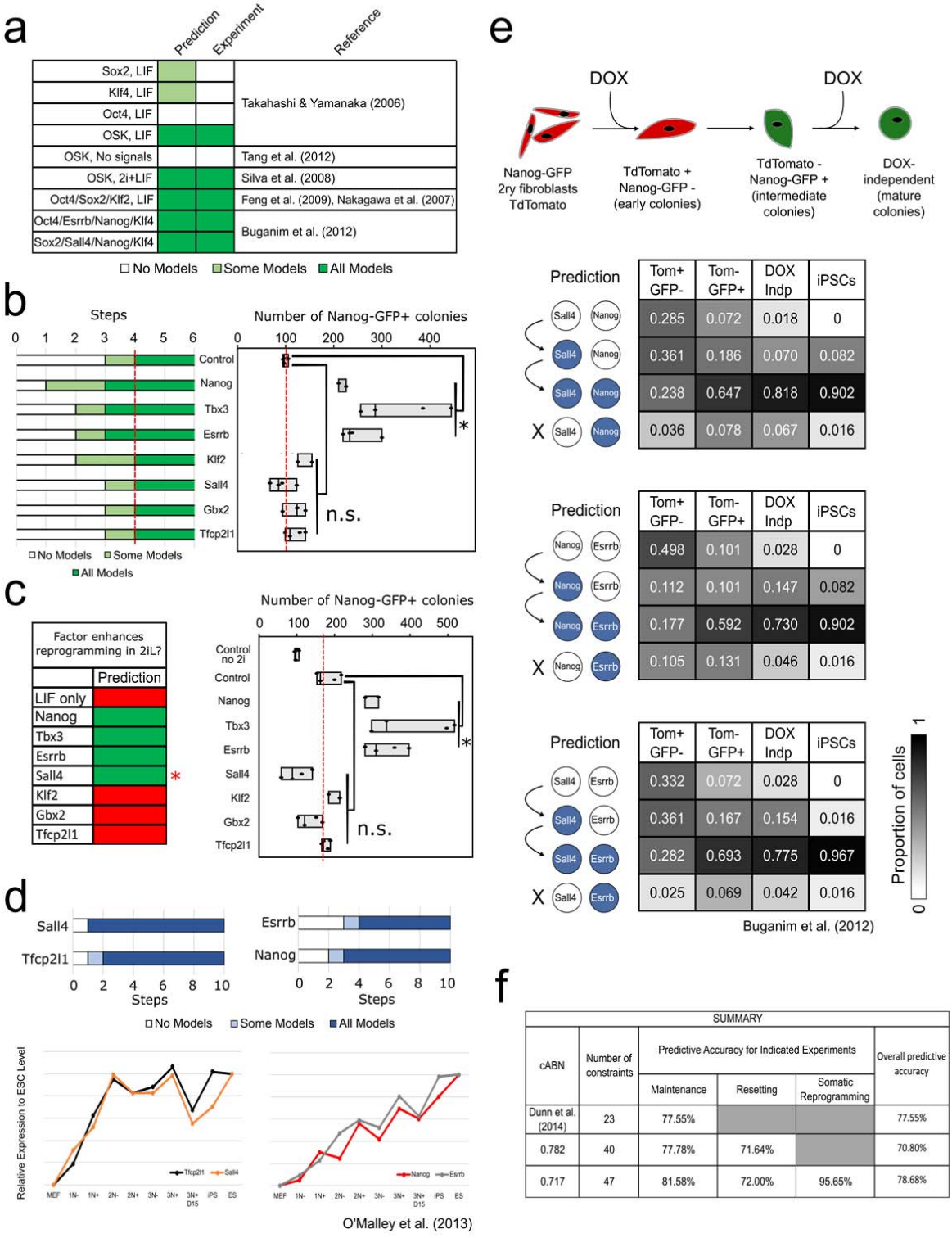

f

SUMMARY					
cABN	Number of constraints	Predictive Accuracy for Indicated Experiments			Overall predictive accuracy
		Maintenance	Resetting	Somatic Reprogramming	
Dunn et al. (2014)	23	77.55%			77.55%
0.782	40	77.78%	71.64%		70.80%
0.717	47	81.58%	72.00%	95.65%	78.68%

Figure 7: A common gene regulatory program governs naïve state maintenance, EpiSC resetting and somatic cell reprogramming. (a) Predictions generated by the 0.717 cABN compared with published data on gene combinations that do (dark green) or do not (white) enable MEF reprogramming. (b) Comparisons on predictions (left) and experimental outcome (right) on the potency of additional network factor in OSKM-driven MEF reprogramming in LIF containing medium. n=4. p-values, Student's t-test, *=p<0.05. n.s.=not significant. Red dash lines indicate empty vector+OSKM level. (c) Comparison of predictions (left) and experimental outcome (right) on the potency of additional network factor in OSKM-driven MEF reprogramming in 2i+LIF. n=4. p-values, Student's t-test, *p<0.05. n.s. not significant. Empty vector+OSKM reprogramming in LIF ("control no 2i") was included as a control for the effect of 2i addition. Red dash lines indicate empty vector+OSKM control level. (d) Recapitulation of the gene activation kinetics in MEF reprogramming. Top, the number of regulation steps required for permanent activation of the indicated gene; Tfcp2l1 and Sall4 are found to activate earlier than Nanog and Esrrb. Bottom, gene expression of indicated factor extracted from O'Malley et al. (2013) for sorted populations of reprogramming intermediates. (e) Delineation of gene activation at single cell level. Top, experimental scheme used in Buganim et al. (2012) for the isolation of reprogramming intermediates which were profiled by single-cell RT-qPCR. Bottom, Comparisons of predictions of the sequence of gene activation between gene pairs (left) along the reprogramming trajectory in OSKM+LIF, compared with experimental measurements extracted from Buganim et al. (2012). Each table shows the percentage of single cells at the indicated stage of reprogramming (column) that have the indicated expression state of the gene pair considered (row). (f) Summary of the predictive accuracy of the three cABNs progressively refined against experimental results, with 0.717 cABN having the highest predictive accuracy for each set of the investigation.

Supplementary Figure 1

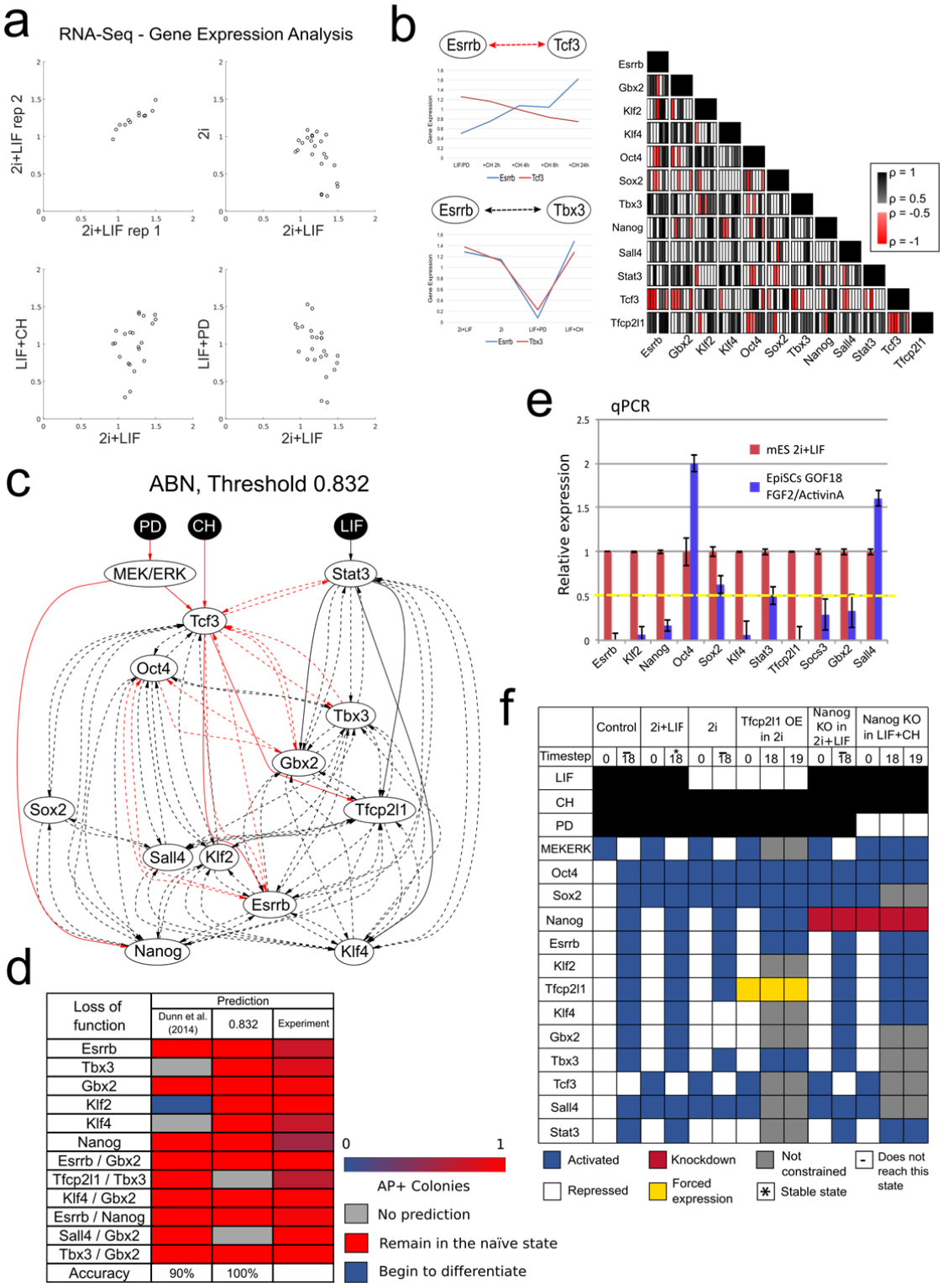

Loss of function	Prediction		
	Dunn et al. (2014)	0.832	Experiment
Esrrb			
Tbx3			
Gbx2			
Klf2			
Klf4			
Nanog			
Esrrb / Gbx2			
Tfcp2l1 / Tbx3			
Klf4 / Gbx2			
Esrrb / Nanog			
Sall4 / Gbx2			
Tbx3 / Gbx2			
Accuracy	90%	100%	

0 1
AP+ Colonies
No prediction
Remain in the naïve state
Begin to differentiate

Figure S1, related to Fig. 1: Deriving and constraining the 0.832 ABN. (a) RNA-Seq expression data for 12 naive network components, measured in the four possible combinations of LIF, CH and PD. (b) Left, gene expression correlation between gene pairs used to infer possible interactions. Strong negative correlation indicates a possible negative interaction; strong positive correlation indicates a possible positive interaction. Correlation does not inform which gene could be the regulator, so possible interactions are bidirectional. Right, Pearson coefficients for each gene pair for six qRT-PCR and one RNA-sequencing expression datasets. Red: negative coefficient below -0.5. Black: positive coefficient above 0.5. (c) The ABN defined by a Pearson correlation threshold of 0.832. This is refined to become the 0.832 cABN (Fig. 1b) once constraints have been imposed, and required and disallowed interactions have been identified. (d) Comparing predictions for the 0.832 cABN against the naive state maintenance cABN derived by Dunn et al. (2014). Here, the predictions correspond to whether an ESC will remain in the self-renewing state under the indicated knockdown. Note an increase in the number of predictions, with incorrect predictions corrected in the refined 0.832 cABN. (e) Relative gene expression of naïve network components in GOF18 EpiSCs compared to ESCs grown in 2i+LIF. The yellow dashed line indicates the threshold used to discretised expression as High or Low. Only genes significantly above the threshold (Oct4, SOx2 and Sall4) were considered High in EpiSCs. (f) Discretisation of gene expression patterns to define the six EpiSC resetting experimental constraints depicted in Fig. 1c. Each constraint consists of an initial (timestep 0) and final state (timestep 18), which is either stable (asterisk) or unreachable (bar). Components may be knocked down (red) or under forced expression (yellow). If a specific gene expression is unknown, it is unconstrained (grey).

Supplementary Figure 2

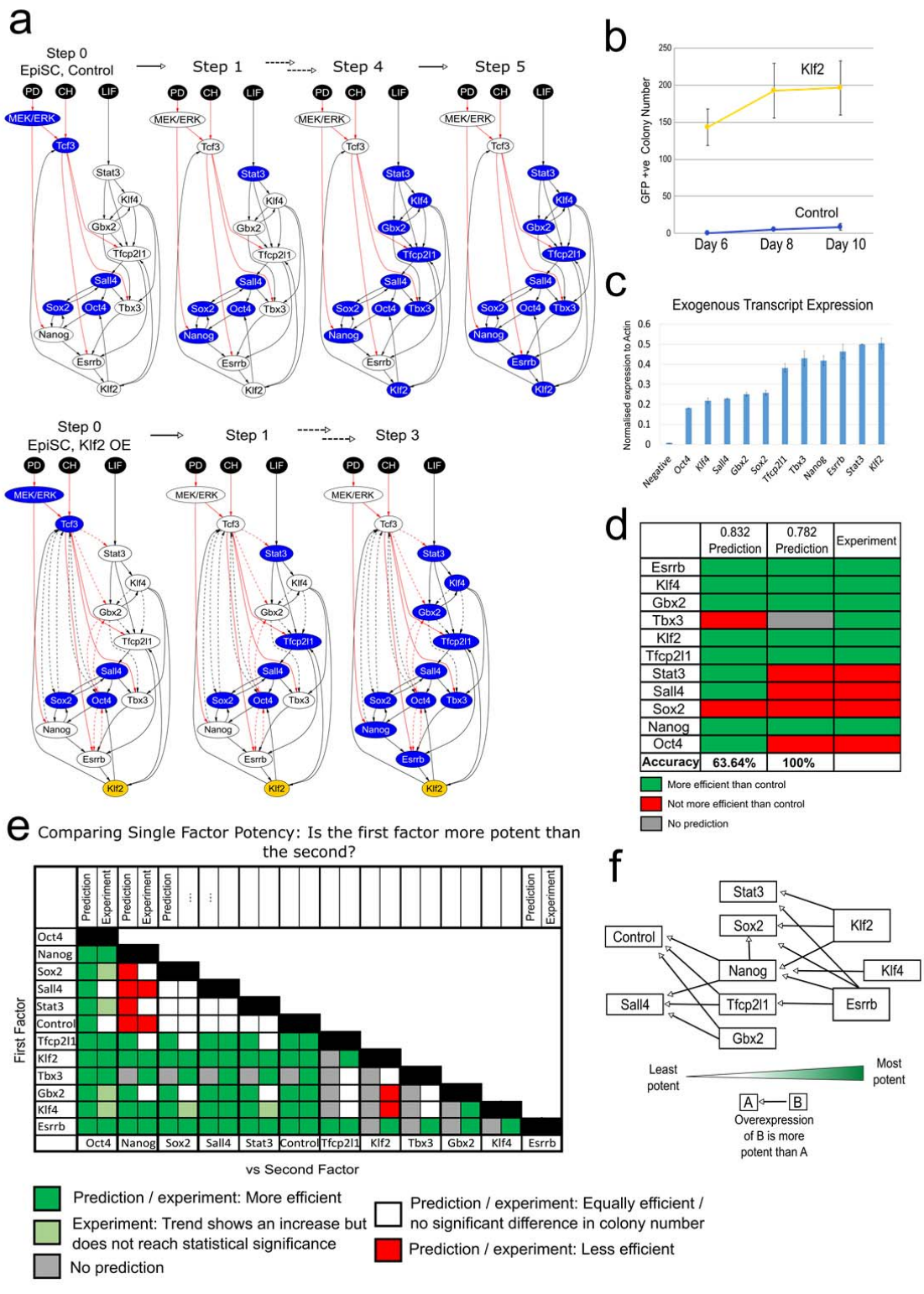

Figure S2, related to Fig. 1: Predicting the relative potency of single factor forced expression in EpiSC resetting. (a) Schematic representation of network progression with forced expression of Klf2, which allows the network to stabilise in the naïve state in fewer steps compared to empty vector control in 2i+LIF (Fig. 1F). (b) Oct4-GFP^{+} colony number measured over the resetting time course under empty vector control and forced Klf2 expression. (c) Expression of exogenous transcription normalised to actinβ. n=3, Mean+/- S.D. (d) A summary of the predictions from the 0.832 and 0.782 cABNs of whether the indicated forced expression was more efficient than empty vector control, compared with experiment. The predictive accuracy of the models increases in the 0.782 cABN. (e) Comparison summary between predictions and experimental results on resetting potency between gene pairs. Each row compares the prediction from the 0.782 cABN (left box) with experiment (right box), showing whether the first factor (row) is more/less potent (green/red) than the second factor (column). We show experimental results where there was a significant difference between the resulting colony number (Student's t-test, $p<0.05$). In none of the cases tested were the predictions in disagreement with the experimental results (i.e. prediction of gene X being more efficient than gene Y, when in fact gene Y was significantly more efficient than X). (f) Schematic summary of (e), illustrating the relative potency between individual factors confirmed by experiment, where the arrow points from a more potent to a less potent factor.

Supplementary Figure 3

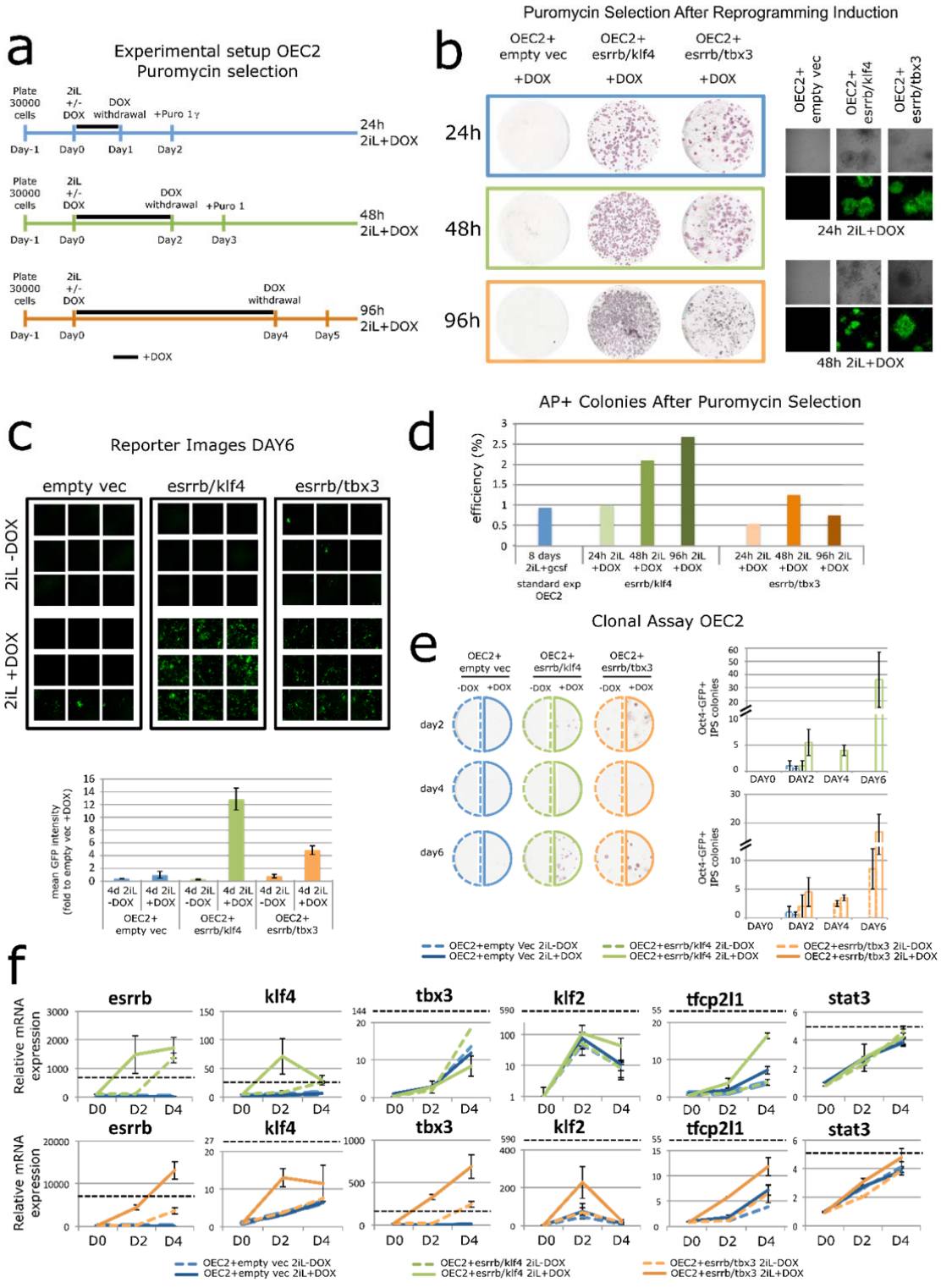

Figure S3, related to Fig. 3: Investigating dual factor expression in OEC2-GY118 EpiSCs. (a) Experimental scheme for the functional characterisation of Esrrb-T2A-Klf4 or Esrrb-T2A-Tbx3 forced expression in OEC2 EpiSC resetting. (b) Left: Representative images of AP staining of reset colonies generated from OEC2 Y118 EpiSCs stably transfected with a piggyBac empty vector or with a piggyBac vector harbouring Esrrb-T2A-Klf4 or Esrrb-T2A-Tbx3. Cells were treated with 2i+LIF to induce resetting and with DOX for 24h, 48h and 96h (grey, green and orange boxes) to induce transgene expression. Puromycin selection was applied 24 hours after DOX withdrawal and AP staining performed at day 8 of resetting. Right: Representative confocal images of Puromycin selected Oct4-GFP^{+} colonies from 1 or 2 days of DOX treatment. (c) Representative confocal images (top) and Oct4-GFP mean intensity quantification (bottom) of OEC2 Y118 EpiSCs expressing Esrrb-T2A-Klf4, Esrrb-T2A-Tbx3 or the empty vector control at day6 of resetting. Mean +/- SEM, n=2. (d) Percentage of AP^{+} colonies in each condition relative to the control treatment (blue), which was in 2i with GCSF for 8 days. Cells expressing Esrrb-T2A-Klf4 (green) or Esrrb-T2A-Tbx3 (orange) were treated with 2i+LIF and DOX for 1, 2 or 4 days represented by light, medium and dark green respectively. One representative experiment is shown. (e) Left: Representative images of AP staining of colonies generated from resetting OEC2 Y118 EpiSCs stably transfected with an empty vector (blue) or with a piggyBac vector containing Esrrb-T2A-Klf4 (green) or Esrrb-T2A-Tbx3 (orange). Cells were treated with 2i+LIF with or without DOX for 2/4/6/8 days (dashed versus solid line), and were subsequently replated at a density of 300 cells/well and cultured for 8 to 10 days in 2i+LIF. Right: Quantification of number of AP^{+} colonies generated from clonal assay performed at day2/4/6/8 of reprogramming of Esrrb-T2A-Klf4 (top) and Esrrb-T2A-Tbx3 (bottom) expressing cells. Mean +/- SEM, n=2. (f) Relative expression of network components in F/A, at day 2 and 4 of resetting in the presence or absence of DOX. Black dashed line indicates expression levels in mouse ESCs maintained in 2i+LIF. Gapdh served as an internal control. Mean +/- SEM, n=2.

Supplementary Figure 4

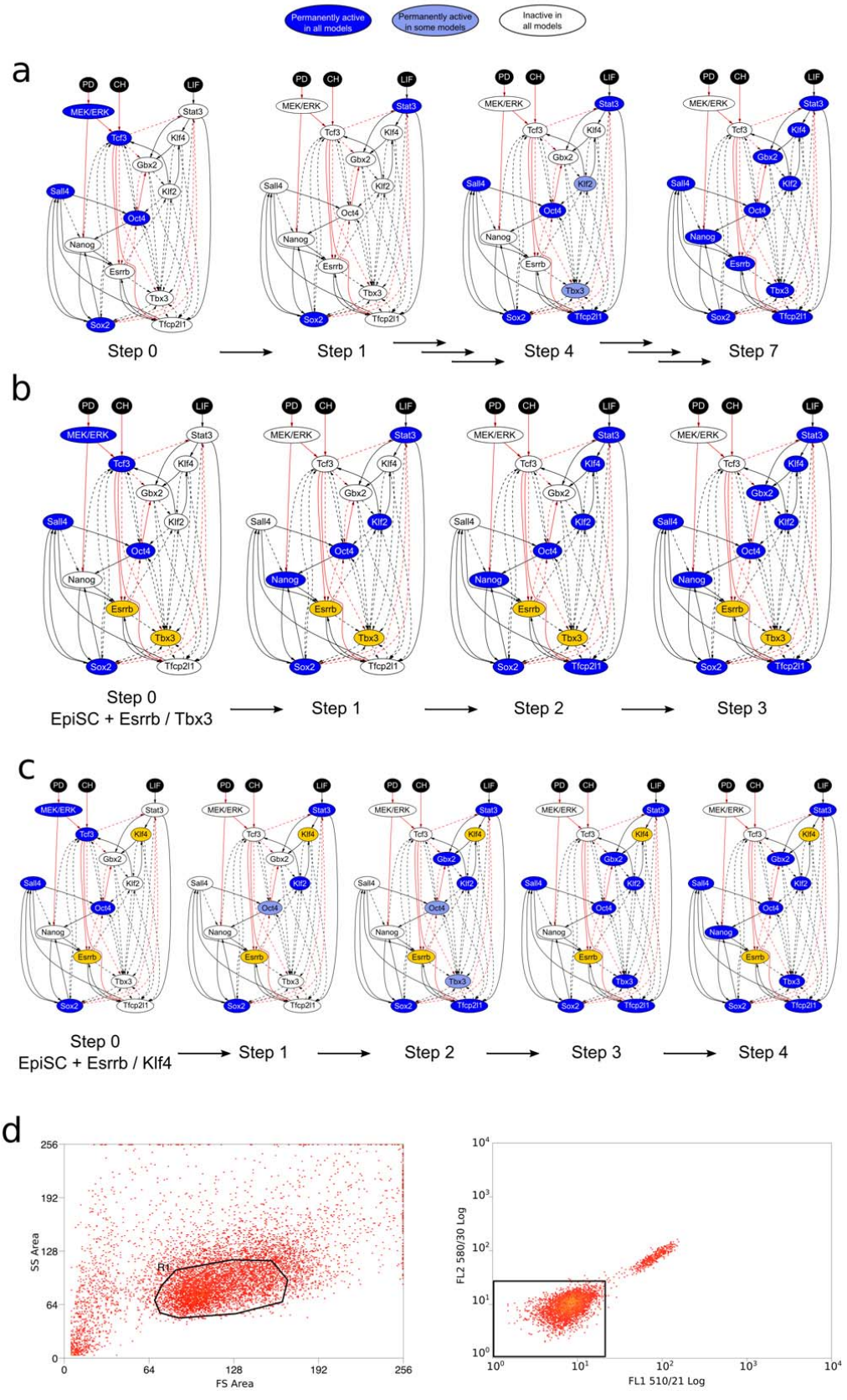

Figure S4, related to Fig. 3 and Fig. 4a, b: A comparison of the resetting kinetics under empty vector control and dual factor expression, visualised on the 0.782 cABN. (a) Resetting under 2i+LIF alone, which takes 7 steps to stabilise in the naïve state. (b) Resetting under dual expression of Esrrb and Tbx3 in 2i+LIF, which takes 3 steps to stabilise in the naïve state. (c) Resetting under dual expression of Esrrb and Klf4 in 2i+LIF, which takes 4 steps to stabilise in the naïve state. (d) Gates used in the FACS experiments described in Fig 4 d. First, individual cells were separated from debris and small cell clusters using Forward Scatter Area vs Side Scatter Area (left), then we identified GFP/Venus negative cells by looking at the level of fluorescence at 510/21 nm using uninduced E/K-EpiSCs. Gates used to sort GFP/Venus positive cells are indicated in Fig. 4d.

Supplementary Figure 5

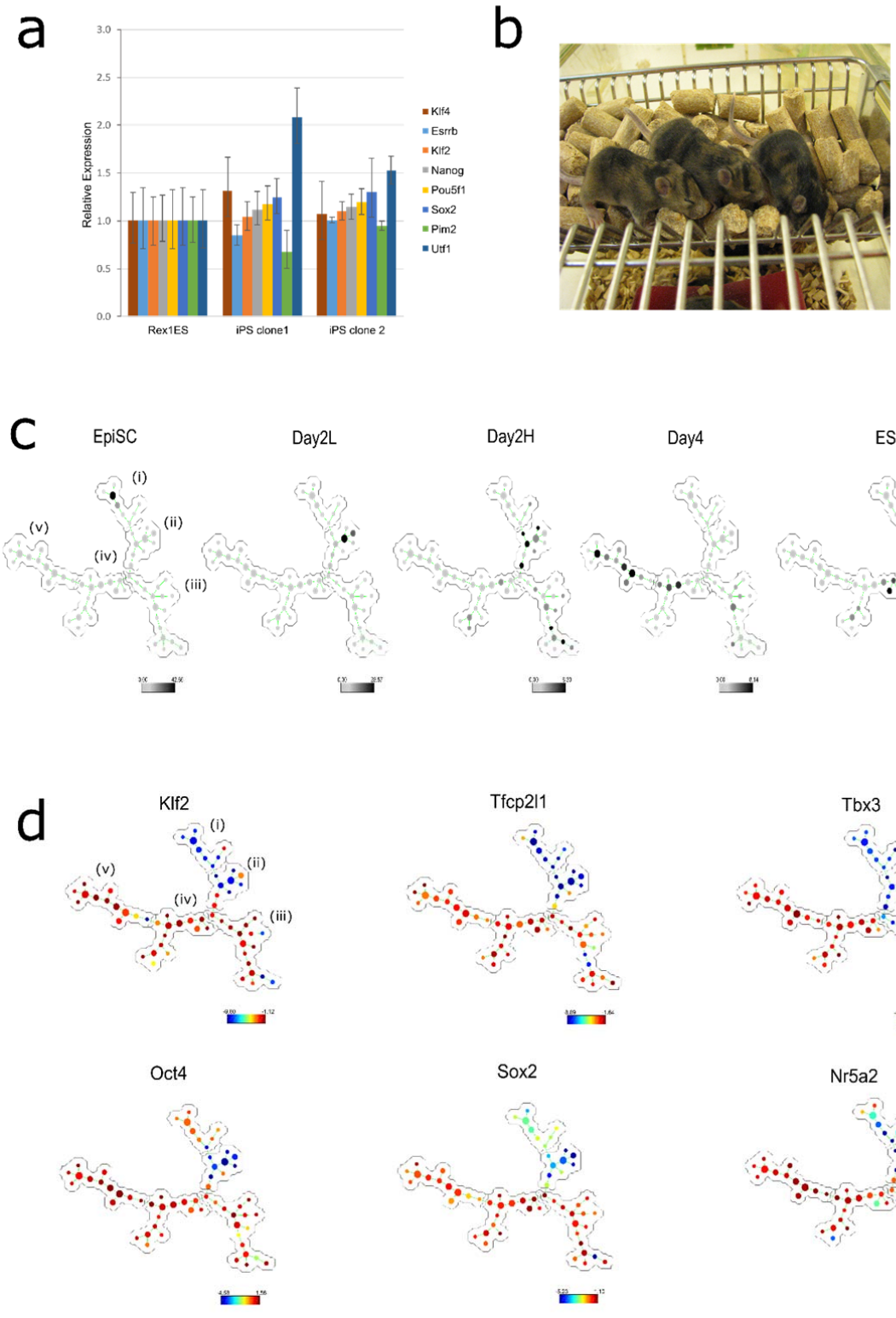

Figure S5, related to Figs. 4 and 5: Analysis of resetting time course using SPADE and clones generated by forced expression of Esrrb-T2A-Klf4 for 4 days. (a) Expression of naïve and early differentiation markers is comparable in Rex1-GFP mESCs and Day4 high cells cultured in 2i+LIF without DOX after 3 passages. (b) Contribution to adult chimeras after blastocyst injection of reset clones confirming the naïve pluripotent identity after resetting by Esrrb/Klf4 dual expression. (c) Clustering of cells from each time points in SPADE tree. Each dot represents a group of cells with the size reflecting cell density. Cells from each time point predominantly, but not exclusively cluster with a branch of the tree, with five populations progress from EpiSCs (branch i) to Day4 high (branch v). (d) SPADE analysis of single cell gene expression of naïve network components along the resetting trajectory, where clusters are coloured according to the expression of the indicated factor.

Supplementary Figure 6

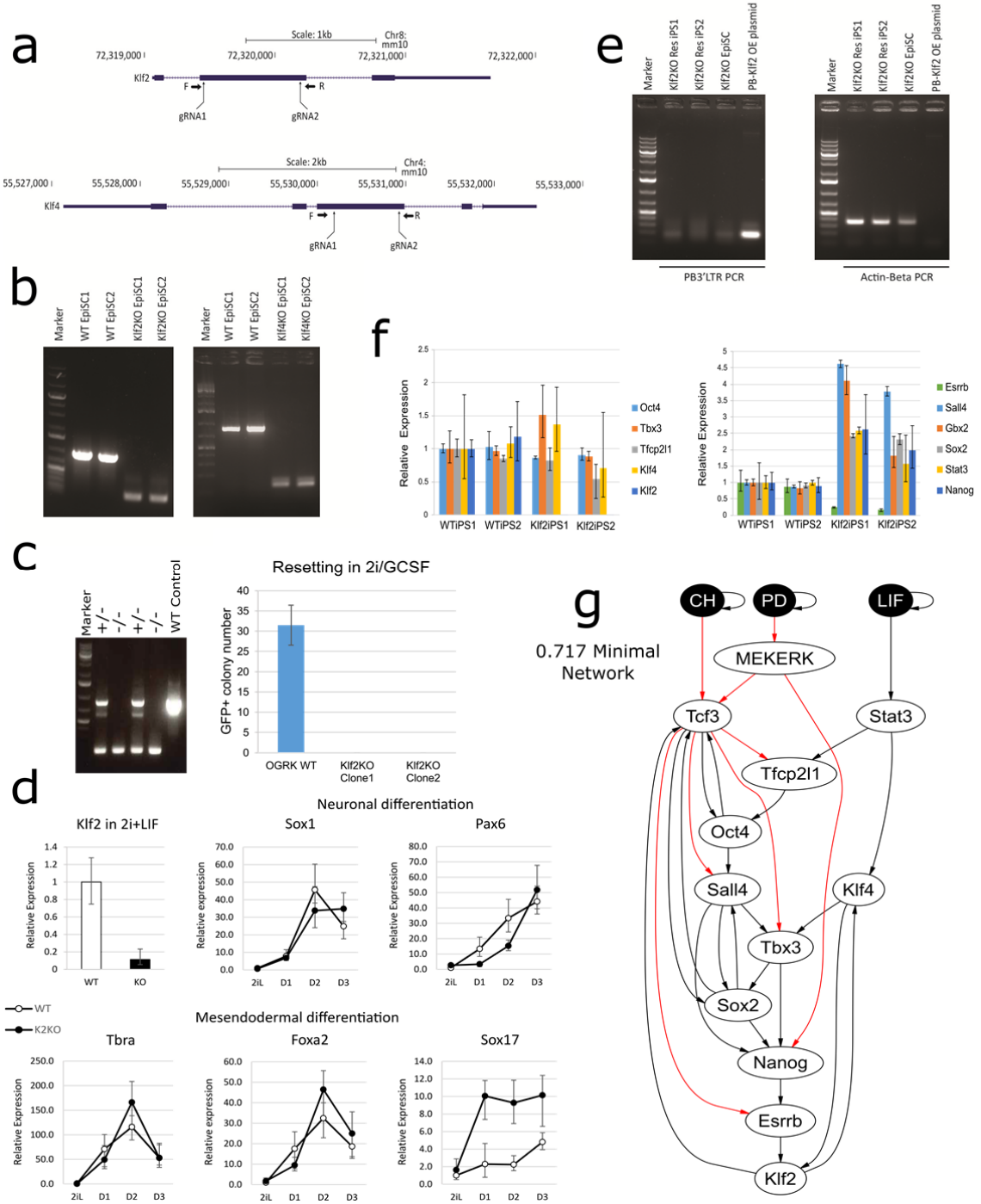

Figure S6, related to Fig. 6: Klf2 and Klf4 KO EpiSC generation and transgene free Klf2KO iPSCs. (a) Strategies for generating Klf2 and Klf4 KO GOF18 EpiSCs using CRISPR/Cas9. Two guide RNAs were designed to flank the largest coding exons for each gene. (b) Genotyping confirmation for homozygous deletion of Klf2 (left) and Klf4 (right) mutants in two independent clones. (c) We derived a new EpiSC line (OGRK) from E5.5 embryo using N2B27 medium supplemented with ActivinA/Fgf2/Xav939 on Fibronectin, which does not reset spontaneously in 2i+LIF. Stable expression of a chimeric GCSF/LIF GY118F receptor (Yang et al., 2010) allows resetting in the presence of 2i+GCSF. We generated Klf2 KO OGRK lines with the strategy described in panel (a) (left) and observed that in the absence of Klf2, resetting was abolished (right), as observed in GOF18 EpiSCs. (d) Gene expression of differentiation markers in wild type and Klf2 KO ES cells generated as in (a). Cells were exposed to monolayer differentiation protocols for neuroectoderm and mesoendoderm (as described in Mulas et al., 2017) and analyses every 24 hours for 3 days. The values are normalised to wild type ES cells in 2i+LIF and Actβ is used as the internal reference. Mean+/-SD, n=2. (e) Klf2KO reset cells generated by transgene overexpression do not contain the transgene stable integration, as demonstrated by the genomic PCR detecting transgene plasmid backbone fragment PB3'LTR (left). ActB genomic PCR (right) serves as a PCR control. (f) Gene expression of naïve and transition markers in transgene free iPSCs derived from WT and Klf2KO EpiSCs after 3 passages. n=3, Mean+/-SD. (g) minimal model within the 0.717 cABN.

Supplementary Figure 7

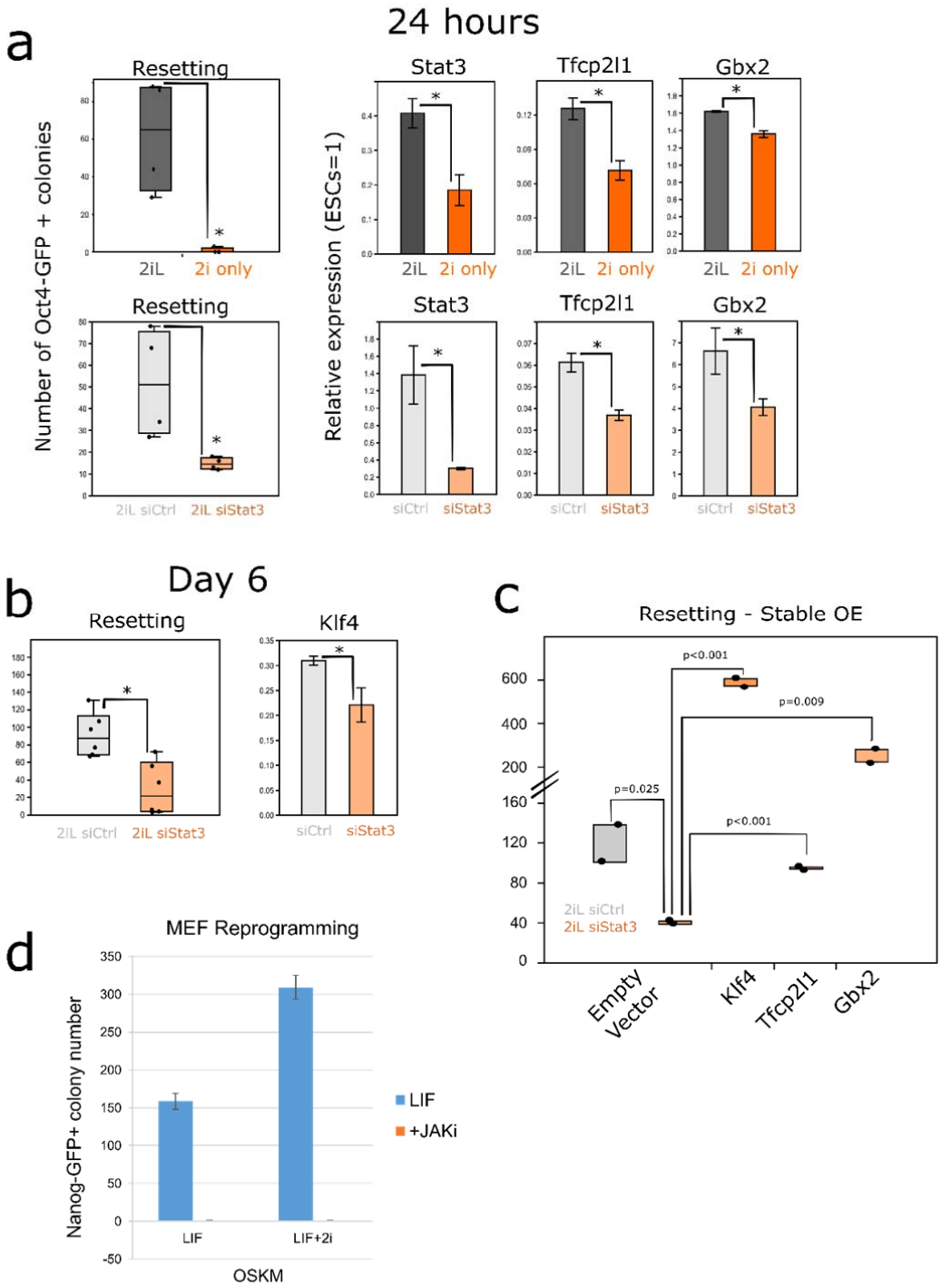

Figure S7, related to Fig. 7: Investigation of stat3 downstream effectors in EpiSC resetting (a-c, related to Fig 6), and LIF requirement in MEF reprogramming. (a) Left, EpiSC resetting efficiency measured by Oct4-GFP^{+} colony formation in 2i alone, or upon Stat3 knockdown compared to 2i+LIF. n=4, Mean+/-SD. *: p-value<0.05, Student's t-test. Right, induction of Stat3, Tfcp2l1 and Gbx2 expression was impeded in 2i alone or Stat3 knockdown in 2i+LIF at 24 hour EpiSC resetting. n=3, Mean+/-SD. *: p-value<0.05, Student's t-test. (b) Reduction of Klf4 expression was observed at day 6 resetting upon Stat3 knockdown. (c) Effect of Stat3 knockdown in Oct4-GFP^{+} colony formation capacity of GOF18 EpiSCs stably overexpressing Tfcp2l1, Gbx2 or Klf4 individually. n=2, Mean+/-SD. p-value indicated, Student's t-test. (d) Nanog-GFP+ iPSC formation in OSKM-driven MEF reprogramming in the presence or absence of LIF signalling inhibitor Jaki. n=2, Mean+/-SD.